Mass transfer at two-phase and three-phase interfaces

A. Weber, R. Darling, J. Meyers and J. Newman

Volume 1, Part 2, pp 47–69

in

Handbook of Fuel Cells – Fundamentals, Technology and Applications
(ISBN: 0-471-49926-9)

Edited by

Wolf Vielstich
Arnold Lamm
Hubert A. Gasteiger

Chapter 7

Mass transfer at two-phase and three-phase interfaces

A. Weber[1], R. Darling[2], J. Meyers[2] and J. Newman[1]

[1] *University of California, Berkeley, CA, USA*
[2] *UTC Fuel Cells, South Windsor, CT, USA*

1 INTRODUCTION

Mass transport losses represent a significant inefficiency in fuel cell systems. In fuel cells, the major mass transport losses are associated with the transport of charged and uncharged species in the electrolytic phase and the transport of gas phase reactants and products. The causes for these losses and their mathematical descriptions are the principal issues discussed in this chapter. Other mass transport related processes, such as catalyst sintering and membrane poisoning, may also affect fuel cell performance. In this review, we consider only the effects of mass transport that pertain to the movement of critical reactants and products. This chapter begins with a simplified model of a fuel cell that introduces many of the key components. This is followed by brief descriptions of porous electrode theory, gas phase mass transport, convective transport of liquids, transport in electrolytic solutions, and numerical simulations of the cathode of a proton exchange membrane (PEM) fuel cell.

Figure 1 shows a cross-sectional view of a PEM fuel cell operating on reformed hydrocarbon fuel and air. Table 1 gives typical through-plane dimensions for the various components. The membrane area may range from $1\,\mathrm{cm}^2$ for a lab-scale unit to $1\,\mathrm{m}^2$ for an automotive or stationary power plant. All types of fuel cells discussed in this chapter contain similar components, the major difference being the nature of the electrolyte. Commonly encountered fuel cell electrolytes include phosphoric acid, potassium hydroxide, cation exchange membranes, molten carbonate, and solid oxides.

The fuel is fed into the anode flow field, moves through the diffusion medium, and reacts electrochemically at the anode catalyst layer. The diffusion medium is typically a carbon cloth or carbon paper, possibly treated with Teflon®. The catalyst layer usually contains a platinum alloy supported on carbon and an ionomeric membrane material such as Nafion®. For an acid fuel cell operating with hydrogen as the fuel, the hydrogen oxidizes according to the reaction

$$\mathrm{H_2} \longrightarrow 2\mathrm{H^+} + 2\mathrm{e^-} \tag{1}$$

The oxidant, usually oxygen in air, is fed into the cathode flow field, moves through the diffusion medium, and is reduced at the cathode according to the reaction

$$4\mathrm{H^+} + 4\mathrm{e^-} + \mathrm{O_2} \longrightarrow 2\mathrm{H_2O} \tag{2}$$

The water, either liquid or vapor, produced by the reduction of oxygen at the cathode exits the fuel cell through either the cathode or the anode flow field. This movement must be accomplished without hindering the transport of reactants to the catalyst layers in order for the fuel cell to operate efficiently. Adding equations (1) and (2) yields the overall reaction

$$2\mathrm{H_2} + \mathrm{O_2} \longrightarrow 2\mathrm{H_2O} \tag{3}$$

Handbook of Fuel Cells – Fundamentals, Technology and Applications, Edited by Wolf Vielstich, Hubert A. Gasteiger, Arnold Lamm. Volume 1: *Fundamentals and Survey of Systems*. ISBN: 0-471-49926-9.

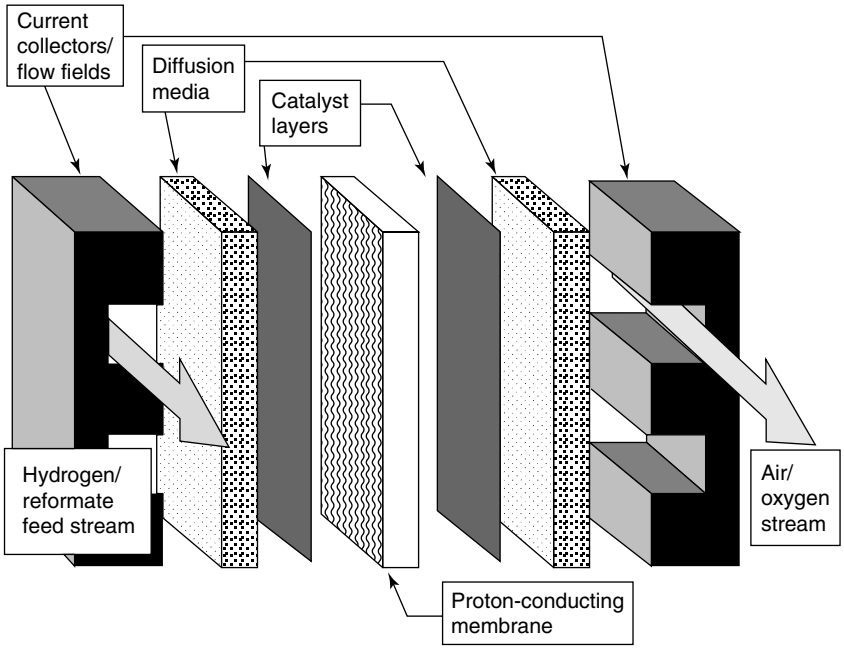

Figure 1. Schematic diagram of a hydrogen polymer electrolyte membrane fuel cell.

Table 1. Thickness of fuel cell components.

Component	Thickness (μm)	Reference
Flow channel	3000	40
Diffusion medium	100–300	43
Catalyst layer	5–25	10
Membrane	10–200	40

The electrons generated at the anode pass through an external circuit and may be used to perform work before they are consumed at the cathode. The maximum work that the fuel cell can deliver may be found by considering the theoretical open-circuit potential of the cell. A typical PEM cell can be represented as

$$\begin{array}{c|c:c:c|c} \alpha & \beta & \gamma & \beta' & \alpha' \\ \text{Graphite} & \begin{array}{c}\text{Pt}_{(s)}, \text{H}_{2(g)} \\ \text{H}_2\text{O}_{(g)}\end{array} & \begin{array}{c}\text{Membrane} \\ \text{H}^+_{(m)}, \text{H}_2\text{O}_{(m)}\end{array} & \begin{array}{c}\text{Pt}_{(s)}, \text{O}_{2(g)} \\ \text{H}_2\text{O}_{(g)}\end{array} & \text{Graphite} \end{array} \qquad (4)$$

where each Greek letter identifies a distinct phase and the wavy lines imply that the membrane phase boundary is not sharp; rather, the membrane extends into adjacent regions and may include water activity gradients. The potential of this cell is

$$FU = -F(\Phi^{\alpha} - \Phi^{\alpha'}) = \mu_{e^-}^{\alpha} - \mu_{e^-}^{\alpha'} \qquad (5)$$

where F is Faraday's constant, U is the thermodynamically defined reversible cell potential, Φ^{α} is the electrical potential of phase α, and $\mu_{e^-}^{\alpha}$ is the electrochemical potential of electrons in phase α. After introducing expressions for the activities of the various components, this becomes

$$FU = FU^{\theta} + \frac{RT}{2}\ln a_{\text{H}_2}^{\beta} + \frac{RT}{4}\ln a_{\text{O}_2}^{\beta'} - \frac{RT}{2}\ln a_{\text{H}_2\text{O}}^{\beta'} + (\mu_{\text{H}^+}^{\beta} - \mu_{\text{H}^+}^{\beta'}) \qquad (6)$$

where a_i^{β} is the activity of species i in phase β, R is the ideal gas constant, T is the absolute temperature, and U^{θ} is the standard cell potential, a combination of appropriately chosen reference states. This equation reduces to the familiar Nernst equation when the gases are assumed to be ideal and activity gradients in the electrolyte are neglected.

1.1 Introductory model

A good way to introduce the subject is to begin with a simple steady state model that captures the gross behavior of a fuel cell. For our example, we consider a phosphoric acid fuel cell operating on a reformed hydrocarbon fuel and air at atmospheric pressure and a temperature of 190 °C. If the fuel and air streams flow cocurrently, and all of the product water leaves with the air stream, then it is possible to relate the gas compositions in the two flow channels

to the fuel utilization by means of material balances and Faraday's law. The hydrogen utilization at any point along the channel can be defined as

$$u = \frac{X^0_{H_2} - X_{H_2}}{X^0_{H_2}} \tag{7}$$

where X_{H_2} is the molar flow rate of hydrogen divided by the molar flow rate of inerts, principally carbon dioxide, in the fuel stream. The superscript 0 denotes the value at the inlet of the flow field. Faraday's law can then be used to relate the amount of hydrogen reacted to the current

$$\frac{d}{dy}(X_{H_2} F_a) = -\frac{iW}{2F} \tag{8}$$

where i is the local current density, W is the width perpendicular to the flow, y is the distance down the flow field channel, and F_a is the molar flow rate of inerts at the anode. Similar expressions can be written for water and oxygen at the cathode. Using the reaction stoichiometry and Faraday's law, we get

$$X^0_{H_2} u = (X_{H_2O} - X^0_{H_2O}) f = 2(X^0_{O_2} - X_{O_2}) f \tag{9}$$

where X_i is the ratio of moles of component i to moles of inerts in the same stream and f is the ratio of moles of inerts in the air stream to moles of inerts in the fuel stream. The first equality arises directly from our assumption that all of the product water exits the fuel cell in the air stream. While this assumption is not generally true, it does serve as a useful starting point. Thus, the gas compositions in the flow channel are entirely determined by u, f, and the inlet gas composition; such a simple relationship is impossible when the gases are not fed cocurrently. However, this analysis should provide a reasonable approximation of the true behavior when one of the electrodes is limiting. Figure 2 shows the mole fractions when a dry, equimolar mixture of hydrogen and carbon dioxide is fed to the anode, and dry air, 20% in excess of the stoichiometric amount, is fed to the cathode. In practice, performance gains due to adding more air must be balanced against the costs and parasitic power losses of pumping the air.

Figure 3 shows a typical fuel cell polarization curve. The curve includes a sharp drop in potential at low current densities due to the sluggish kinetics of the oxygen reduction reaction (ORR). This part of the polarization curve is commonly called the kinetic regime. At moderate current densities, the cell enters an ohmic regime where the cell potential varies nearly linearly with current density. At high current densities, mass transport resistance dominates, and the potential of the cell declines rapidly as the concentration

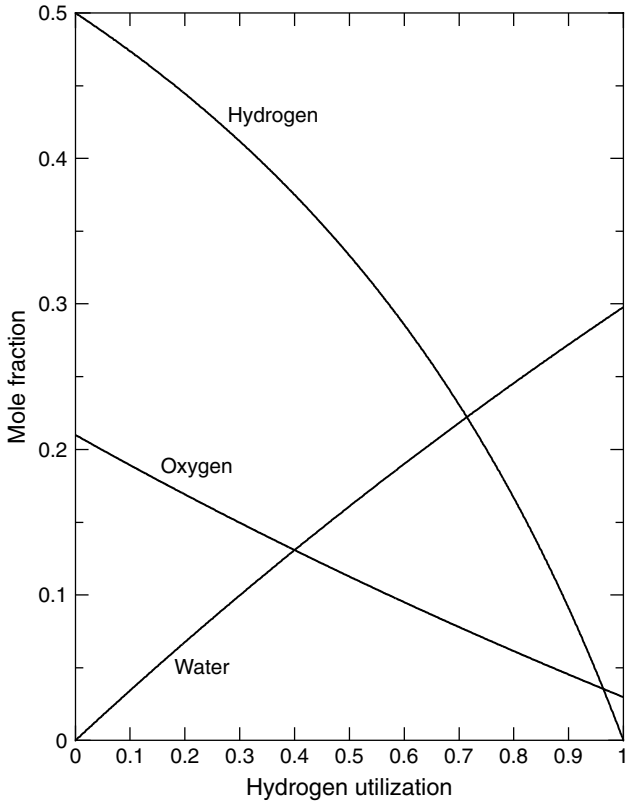

Figure 2. Composition of gas streams. The feed is 50% hydrogen in carbon dioxide, 20% excess air, and $f = 2$.

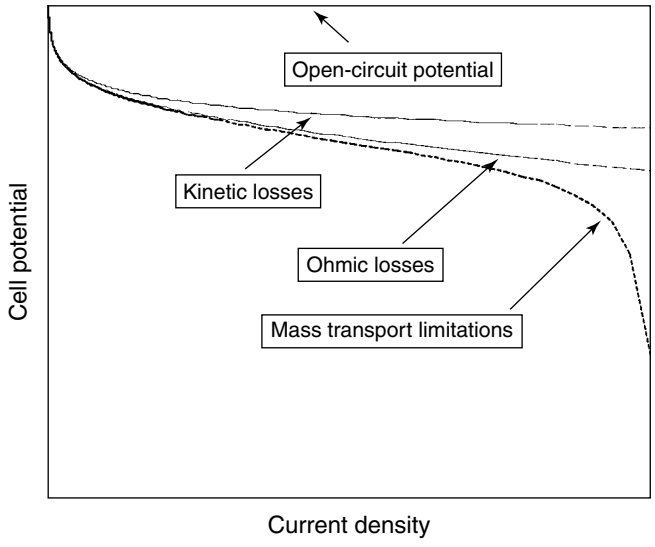

Figure 3. Example of a polarization curve showing the losses associated with irreversibilities in a fuel cell.

of one of the reactants approaches zero at the corresponding catalyst layer. This defines the limiting reactant. In a typical PEM cell operating at temperatures below 80 °C, much of the water produced by the ORR is liquid, and this

liquid water may flood parts of the fuel cell, dramatically increasing the resistance to mass transfer.

A simplified equation[1] describing the major features of a typical polarization curve is

$$V = U^{\theta} + \frac{RT}{\alpha F}\ln(ai_0L) - \frac{RT}{\alpha F}\ln\left(\frac{i}{p_{O_2}}\right) + \frac{RT}{2F}\ln(p_{H_2}) - R'i \tag{10}$$

where V is the cell potential and i is the superficial current density. The first term in the equation, U^{θ}, is the standard cell potential, 1.144 V at 190 °C. The second and third terms arise from the assumption that the ORR follows Tafel kinetics, with a first-order dependence on the partial pressure of oxygen. α is the cathodic transfer coefficient, which normally has a value of 1, a is the interfacial area of the catalyst per unit volume of electrode, i_0 is the exchange current density of the ORR, and L is the thickness of the cathode catalyst layer. Thus, the quantity aL is a roughness factor, a ratio of catalyst area to superficial electrode area. The first and second terms may be combined to form a potential intercept, U'; this quantity is a convenient way to group terms pertaining to (possibly unknown) thermodynamic and kinetic constants. The third term describes the potential loss at the cathode at the specified current density i, and subject to the oxygen partial pressure present at the electrode interface. The fourth term is an equilibrium expression for the hydrogen oxidation reaction (HOR). This is usually a good approximation unless the anode catalyst is poisoned. Finally, R' is the effective ohmic resistance, which includes the resistance of the separator as well as the residual contact resistances between cell components. The detailed reaction rate distributions within the porous electrodes are neglected in this analysis, and the electrodes are treated as planar with enhanced surface area.

The use of equation (10) requires that interfacial partial pressures of oxygen and hydrogen be known. These partial pressures will be lower than those in the channels because of mass transport losses in the backing layers. Conversely, the partial pressure of water will be higher at the cathode catalyst layer than in the cathode gas channel.

At sufficiently high utilizations near the exit of the anode flow channel, hydrogen will be a minor component in the anode fuel stream and, under these conditions, diffusion of hydrogen through the stagnant inert gases in the diffusion layer can be modeled with Fick's law. If we define the limiting current as the current density at which the hydrogen partial pressure goes to zero at the anode catalyst layer, then rearrangement of Fick's law yields

$$x_{H_2}^{i} = x_{H_2}^{b}\left(1 - \frac{i}{i_{\mathrm{lim},H_2}}\right) \tag{11}$$

where x_{H_2} is the mole fraction of hydrogen, and the superscripts i and b refer to the catalyst layer interface and bulk, respectively. The hydrogen limiting current varies with utilization according to

$$i_{\mathrm{lim},H_2} = \frac{2FD_{H_2,CO_2}X_{H_2}^{0}p}{RT\delta}\frac{1-u}{1+X_{H_2}^{0}(1-u)} \tag{12}$$

where $D_{i,j}$ is the diffusion coefficient for species i moving through species j, p is the total gas pressure, and δ is the diffusion length. As a reference, using values given by Newman,[1] the limiting current is 43.2 A cm^{-2} at zero utilization and 1.69 A cm^{-2} at 98% utilization with an equimolar feed of hydrogen and carbon dioxide.

In the cathode diffusion medium, oxygen diffuses through stagnant nitrogen and counter diffusing water vapor. The Stefan–Maxwell equations are appropriate for describing this process. An analytic solution is possible for a three-component system like that described here; see, for example, Bird *et al.*[2]

Figure 4 shows polarization curves at various hydrogen utilizations, using the parameters $U' = 0.694$ V and $R' = 0.278\,\Omega\,\mathrm{cm}^2$. As the hydrogen utilization increases, the partial pressure of hydrogen in the gas channel drops and the effects of mass transfer resistance increase. As specified in equation (9), and under the conditions of cocurrent flow, oxygen utilization and, hence, oxygen mass transport limitations, increase along with hydrogen utilization. The limiting currents in figure 4 are caused by the oxygen partial pressure going to zero at the cathode catalyst layer. Thus, oxygen is the limiting reactant and the introduction of additional oxygen should be considered.

Figure 5 shows the current density as a function of hydrogen utilization at three different cell potentials. Again we see that the performance of the cell decreases as the partial pressures of the reactants drop. Since, during normal operation, the cell potential remains uniform along the flow channel, even as hydrogen and oxygen are being consumed, Figure 5 also indicates how the local current density decreases with position as the air and fuel flow through the cell.

In the remainder of this chapter, we focus on transport processes in the direction normal to the face of the electrodes. Many of the key drivers of cell performance are controlled by the motion of gases and ions across the thickness of the cell, and a great deal of information about factors limiting cell performance might be gleaned by modeling

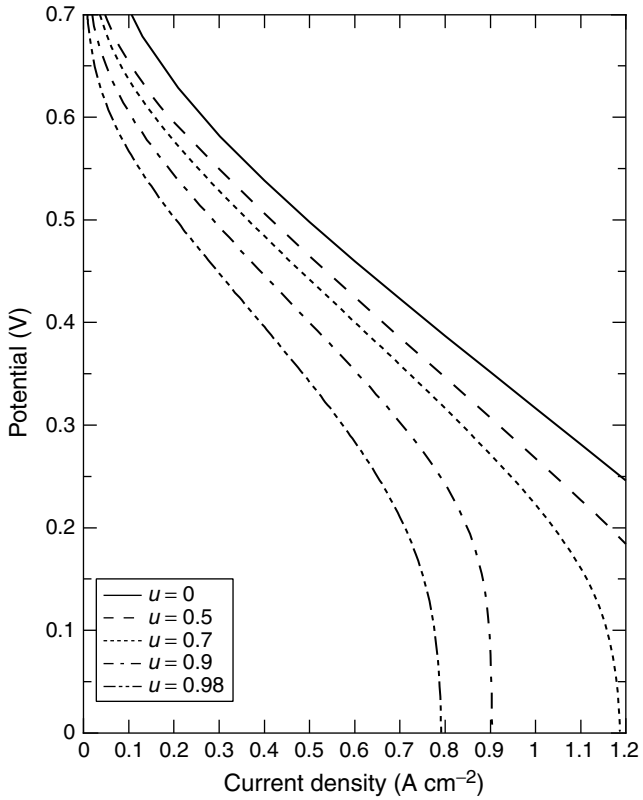

Figure 4. Polarization curves at hydrogen utilizations of 0, 0.5, 0.7, 0.9, and 0.98; calculated using the introductory model.

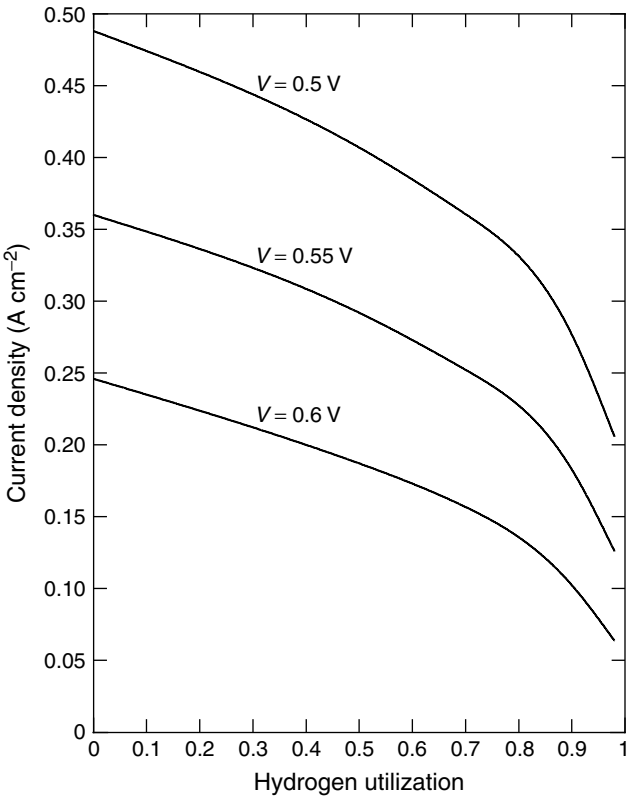

Figure 5. Current density across a cell at three constant cell potentials as a function of hydrogen utilization; calculated using the introductory model.

one-dimensional transport through the various layers. When the resistance to transport across the cell is much greater than the mass transport resistance along the channel, one can decouple the two spatial dimensions and integrate down the channel to determine the cell performance in a manner similar to that set forth above.

2 POROUS ELECTRODES

Porous electrodes are used in fuel cells in order to maximize the interfacial area of the catalyst per unit geometric area. In many fuel cells, an electrolytic species and a dissolved gas react on a supported catalyst. Thus, the electrode must be designed to maximize the available catalytic area while minimizing the resistances to mass transport in the electrolytic and gas phases, and the electronic resistance in the solid phase. Clearly, this is a stringent set of requirements. We want to construct a three-dimensional structure with continuous transport paths in multiple phases. Porous electrode theory provides a mathematical framework for modeling these complex electrode structures in terms of well defined macroscopic variables.

The behavior of porous electrodes is inherently more complicated than that of planar electrodes because of the intimate contact between the solid and fluid phases. Reaction rates can vary widely through the depth of the electrode due to the interplay between the ohmic drop in the solid phase, kinetic resistances, and concentration variations in the fluid phases. The number and complexity of interactions occurring make it difficult to develop analytic expressions describing the behavior of porous electrodes except under limiting conditions. Thus, the governing equations must usually be solved numerically.

Porous electrode theory has been used to describe a variety of electrochemical devices including fuel cells, batteries, separation devices, and electrochemical capacitors. In many of these systems, the electrode contains a single solid phase and a single fluid phase. Newman and Tiedemann reviewed the behavior of these flooded porous electrodes.[3] Many fuel cell electrodes, however, contain more than one fluid phase, which introduces additional complications. The classical gas diffusion electrode, for example, contains both an electrolytic phase and a gas phase in addition to the solid, electronically conducting phase. Earlier reviews of gas diffusion electrodes for fuel cells include those of Chizmadzhev *et al.*[4] and Bockris and Srinivasan.[5] This section deals with general aspects of macroscopic porous

electrode theory and does not delve into detailed reaction mechanisms and electrode morphology. These issues should, of course, be considered when constructing a model of a particular system.

2.1 Macroscopic approach

We follow the macroscopic approach for modeling porous electrodes as described by Newman and Tiedemann.[3] In the macroscopic approach, the exact geometric details of the electrode are neglected. Instead, the electrode is treated as a randomly arranged porous structure that can be described by a small number of variables such as porosity and surface area per unit volume. Furthermore, transport properties within the porous structure are averaged over the electrode volume. Averaging is performed over a region that is small compared to the size of the electrode, but large compared to the pore structure. A detailed description of the averaging can be found in Dunning's dissertation.[6] The macroscopic approach to modeling can be contrasted to models based on a geometric description of the pore structure. Many early models of flooded porous electrodes treated the pores as straight cylinders arranged perpendicular to the external face of the electrode. Further examples of this type of approach are the flooded agglomerate models of Giner and Hunter[7] and Iczkowski and Cutlip.[8] These models are frequently used to describe fuel cells, and treat the electrode as a collection of flooded catalyst-containing agglomerates, which are small compared to the size of the electrode and are connected by hydrophobic gas pores.

2.2 Declaration of variables

A useful place to begin the formulation of the model is to determine the number of independent variables. The first consideration is the number of phases present. For example, consider the catalyst layer in a state of the art PEM fuel cell containing a supported platinum-on-carbon (or platinum-alloy-on-carbon) catalyst, a polymeric membrane material, and a void volume. For reference, the primary carbon particles are approximately 40 nm in diameter,[9] and the platinum crystallites are approximately 2 nm in diameter.[10] If we lump the solid phases comprising the supported catalyst together, and treat the polymeric membrane as a single phase, then we end up with four phases: solid, membrane, gas, and liquid. This last phase corresponds to liquid water infiltrating the gas pores. This model differs, conceptually, from those of Bernardi and Verbrugge[11] and Springer *et al.*[12] by explicitly accounting for a void volume containing gas and liquid water. In Bernardi and Verbrugge's model, oxygen and hydrogen within the catalyst layer travel as dissolved species within the ionomer. Springer *et al.* propose a similar picture, but fit the permeability of the catalyst layer to experimental data. The basic mathematics of the different models are fundamentally similar, a strength of the macroscopic approach. Each phase is assumed to be electrically neutral, an idea that we will return to later. We neglect double layer processes in this chapter, although these may be important in the simulation of transient phenomena. If desired, it is possible to include the interfacial regions between the different macroscopic phases as additional phases with negligible volume, but having the ability to store mass.[13]

Now we turn our attention to the number, M, of degrees of freedom that need to be specified. The Gibbs phase rule allows the reduction of an arbitrarily large number of species to a set of independent components of size M

$$M = C - R - P + 2 \tag{13}$$

where C is the number of species, R is the number of equilibrated homogeneous reactions, P is the number of phases, and the 2 indicates the selection of temperature and pressure. If we have unequilibrated reactions, they would not contribute to R, and if we do not assume phase equilibrium (treating mass transfer separately), we would treat each phase separately, taking $P = 1$. If we also treat pressure and temperature separately, say, by fluid mechanics and an energy balance, we would leave off the 2, yielding $C - R - 1$. For a gas phase of three components and no equilibrated reactions, $C - R - 1 = 2$; specify two mole fractions. In phases without charged species, like the gas phase in our PEM example, we do not need an electrical state variable.

As a second example, consider a sulfuric acid electrolyte containing H^+, HSO_4^-, SO_4^{2-}, H_2SO_4, and H_2O. In this case, $C = 5$ and $R = 2$, which yields $N = 2$, interpreted to mean the electric potential and the concentration of sulfuric acid. $R = 2$ implies that we have two equilibrium relationships among the 5 species, one for bisulfate equilibrium and one for sulfuric acid equilibrium. For Nafion®, we have water, membrane, and protons, $C = 3$. Now, $C - R - 1 = 3 - 0 - 1 = 2$; specify water concentration and potential. This approach allows the electrical systems to be handled without exception, by turning that last degree of freedom into an electric state variable, namely, the potential.

In all of these systems, the corresponding number of transport properties required is

$$\frac{N(N-1)}{2} \tag{14}$$

where N is the number of independent species. Newman[14] gives a more complete counting of transport properties, with simple examples, including thermal and electrical variables.

2.3 Average quantities

In the macroscopic approach, the electrode is treated as a superposition of all phases present. Thus, all variables are defined at all positions within the electrode. The concentration of species i in phase k, $c_{i,k}$, is averaged over the pore volume of phase k, ensuring that the concentration profile is continuous entering or leaving the electrode. $\mathbf{N}_{i,k}$ is the superficial flux density of species i in the pores of phase k averaged over the cross-sectional area of the electrode. These averages apply to regions that are large compared to the pore structure, but small compared to regions over which macroscopic variations occur. The interstitial flux density of species i in phase k is

$$\mathbf{N}_{i,k}^{\text{interstitial}} = \frac{\mathbf{N}_{i,k}}{\varepsilon_k} \tag{15}$$

where ε_k is the volume fraction of phase k. This equation assumes that the medium is isotropic. The superficial current density in phase k is

$$\mathbf{i}_k = F \sum_i z_i \mathbf{N}_{i,k} \tag{16}$$

where F is Faraday's constant and z_i is the valence of species i.

2.4 Ohm's law in the solid phase

In many fuel cell systems, the conductivity of the solid phase is much greater than the conductivity of the electrolytic phase. In this case, it is permissible to treat the solid phase potential as a constant. More generally, the transport of current in the solid phase may be treated with Ohm's law:

$$\mathbf{i}_1 = -\sigma \nabla \Phi_1 \tag{17}$$

where σ is the electrical conductivity of the solid. This conductivity may be adjusted for porosity and tortuosity with a Bruggeman[15] correction

$$\sigma = \sigma_0 \varepsilon_1^{1.5} \tag{18}$$

where ε_1 and σ_0 are the volume fraction and the bulk conductivity of the solid phase, respectively. The conductivity will take on some effective value based on the conductivities of the different solid phase materials. For example, many PEM electrodes contain carbon, platinum, and Teflon® (polytetrafluoroethylene) with bulk conductivities of approximately 25, 10^5, and $10^{-4}\,\mathrm{S\,cm^{-1}}$ at 25 °C, respectively.[16] The electronic current will flow through the platinum and carbon phases, and the carbon will effectively determine the conductivity. Bernardi[17] discusses the averaging of the conductivities of electronically conducting phases in a porous electrode. She advocates Maxwell's model, which assumes a continuous phase and several discrete phases. However, the prediction of conductivities of packed bed materials is not fully resolved; thus, experimental values are preferred when available.

2.5 Electrode kinetics

A single electrochemical reaction can be written schematically as

$$\sum_k \sum_i s_{i,k,h} M_i^{z_i} \longrightarrow n_h e^- \tag{19}$$

where $s_{i,k,h}$ is the stoichiometric coefficient of species i, residing in phase k, and participating in electron transfer reaction h, n_h is the number of electrons transferred in reaction h, and $M_i^{z_i}$ represents the chemical formula of i having valence z_i. The electrons reside in the solid phase.

The rate of an electrochemical reaction depends upon the potential drop across the interface and the concentrations of the various species. It is not possible to write down completely general rate equations for electrochemical reactions. However, it is frequently possible to begin with a Butler–Volmer equation.

Two electrochemical reactions of particular interest in fuel cells are the HOR and the ORR. In the absence of catalyst poisons, the HOR is fast, and a detailed reaction mechanism may be unnecessary. Instead, we use a Butler–Volmer equation of the form

$$i = i_0 \left[\frac{p_{\mathrm{H_2}}}{p_{\mathrm{H_2}}^{\mathrm{ref}}} \exp\left(\frac{(1-\beta) n F}{RT} (\Phi_1 - \Phi_2) \right) - \exp\left(\frac{\beta n F}{RT} (\Phi_1 - \Phi_2) \right) \right] \tag{20}$$

where i_0 is the exchange current density per unit catalyst area evaluated at the reference conditions, $n = 2$ is the number of electrons transferred, β is a symmetry factor having a typical value of 0.5, $p_{\mathrm{H_2}}$ is the hydrogen partial pressure, $p_{\mathrm{H_2}}^{\mathrm{ref}}$ is the hydrogen partial pressure at which the exchange current density is specified, typically 1 bar, Φ_1 is the potential in the solid phase, and Φ_2 is the potential in the

proton conducting phase. In this discussion, the potential in the proton conducting phase is measured with a normal hydrogen electrode (NHE), defined as a platinum metal electrode exposed to hydrogen at 1 bar and a solution of 1 N acid, measured at the same temperature as the solution of interest. This kinetic expression reduces to the Nernst relationship when the ratio i/i_0 becomes small. Springer *et al.*[18] present a treatment of the HOR applicable to a platinum catalyst in a PEM fuel cell when carbon monoxide poisoning of the electrode is significant. This treatment involves consideration of the Tafel and Volmer reaction steps.

The ORR, on the other hand, is slow and represents the principal inefficiency in many fuel cells. The ORR behaves irreversibly and may be modeled reasonably well with Tafel kinetics with a first-order dependence upon oxygen partial pressure. Appleby[19] suggests the following form for oxygen reduction in acid electrolytes

$$i_n = -i_0 \left(\frac{p_{O_2}}{p_{O_2}^{\text{ref}}} \right) \exp \left(\frac{-\alpha F}{RT} (\Phi_1 - \Phi_2 - U^{\theta}) \right) \quad (21)$$

where p_{O_2} is the oxygen partial pressure, i_0 is the exchange current density, α is the cathodic transfer coefficient, for which Appleby recommends a value of 1, and U^{θ} is the standard potential for oxygen reduction, 1.229 V at 25 °C. A linear fit on a Tafel plot of surface overpotential, $\eta_s = \Phi_1 - \Phi_2 - U^{\theta}$, versus the log of the current density yields the commonly reported Tafel slope, b

$$b = 2.303 \frac{RT}{\alpha F} \quad (22)$$

Equation (21) is first order in oxygen concentration and applies for acid electrolytes; another form is required for basic electrolytes. Additionally, the rate of the ORR may depend upon proton concentration; see, for example, Kinoshita.[20] Furthermore, the ORR is sensitive to the presence of adsorbed anions and surface oxides on platinum. Finally, one may prefer to use the dissolved oxygen concentration in equation (21) instead of the oxygen partial pressure. Typically, these can be related through Henry's law.

Further refinement of the kinetic expressions may be necessary to describe the effects of competitively adsorbed poisons or unwanted by-products. It is usually possible to incorporate such effects into a general numerical model.

2.6 Material balances

Reactions occurring within the porous electrode are mathematically treated as source or sink terms, rather than as boundary conditions, as reactions at a planar electrode might be treated. It is necessary to write a material balance for each independent component in each phase. In the following discussion, we assume that there is only one solid, electronically conducting phase, denoted by subscript 1. The differential form of the material balance for species i in phase k is

$$\frac{\partial \varepsilon_k c_{i,k}}{\partial t} = -\nabla \cdot \mathbf{N}_{i,k} - \sum_h a_{k,1} s_{i,k,h} \frac{i_{h,k}}{n_h F} + \sum_l s_{i,k,l} \sum_{p \neq k} a_{k,p} r_{l,k-p} + \sum_g s_{i,k,g} R_{g,k} \quad (23)$$

The term on the left side of the equation is the accumulation term, which accounts for the change in the total amount of species i held in phase k within a differential control volume. The first term on the right side of the equation keeps track of the material that enters or leaves the control volume by mass transport. The remaining three terms account for material that is gained or lost due to chemical reactions. The first summation includes all electron transfer reactions that occur at the interface between phase k and the solid, electronically conducting phase. The second summation accounts for all other interfacial reactions that do not include electron transfer, and the final term accounts for homogeneous reactions in phase k.

In the above expression, $c_{i,k}$ is the concentration of species i in phase k, and $s_{i,k,l}$ is the stoichiometric coefficient of species i in phase k participating in heterogeneous reaction l. When we specify $s_{i,k,l}$, we necessarily assume that species i exists in phase k immediately prior to reaction or upon formation. If i can exist in more than one phase, care must be taken to ensure that phase equilibrium is properly addressed. $a_{k,p}$ is the specific surface area (surface area per unit total volume) of the interface between phases k and p. We assume that this is a nonspecific surface area for the interface; for example, if only a particular crystalline surface participates in an interfacial reaction, the portion of the total surface area covered by that particular crystal face must be included in the kinetic rate constants, rather than grouped into the $a_{k,p}$ term. This simplifies the terminology of this discussion considerably. $i_{h,k}$ is the normal anodic interfacial current transferred per unit interfacial area across the interface between the solid, electronically conducting phase and phase k due to electron transfer reaction h. We note that a current $i_{h,k}$, written with two subscripts, implies an interfacial, or transfer, current density. Conversely, a current $\mathbf{i}_k$, written in boldface and with a single subscript, indicates the total current density carried within phase k. This current density is, strictly speaking, a vector quantity. $r_{l,k-p}$ is the rate of the heterogeneous reaction l per unit of interfacial area between phases k and p. $R_{g,k}$ is the rate of a

strictly homogenous reaction g in phase k per unit volume of phase k.

The electron transfer reactions could also be treated as simple interfacial reactions taking place between a given phase and the solid. Faraday's law can be used to relate this reaction rate to the normal transfer current density for reaction h

$$i_{h,k} = n_h F r_{h,k-1} \tag{24}$$

where $r_{h,k-1}$ is the rate of reaction h occurring at the interface between phase k and the solid, electronically conducting phase and $i_{h,k}$ is, as described above, the normal interfacial current density flowing to phase k from the solid phase due to an anodic reaction h.

2.7 Electroneutrality and conservation of charge

Since a large electrical force is required to separate charge over an appreciable distance, a volume element in the electrode will, to a good approximation, be electrically neutral. We further assume that each phase within the electrode is electrically neutral. Thus, for each phase

$$\sum_i z_i c_{i,k} = 0 \tag{25}$$

The assumption of electroneutrality implies that the diffuse double layer, where there is significant charge separation, is small compared to the volume of the electrode, which is normally the case. The assumption of electroneutrality also leads us to the conclusion that the divergence of the total current is zero

$$\sum_k \nabla \cdot \mathbf{i}_k = 0 \tag{26}$$

Using the subscript 1 to again denote the solid, electronically conductive, phase, we may relate the divergence of the electronic current to the rates of the electrochemical reactions. In other words, $-\nabla \cdot \mathbf{i}_1$ represents the total anodic rate of electrochemical reactions per unit volume of electrode. This can be related to the average transfer current density, and when combined with equation (24), yields

$$-\nabla \cdot \mathbf{i}_1 = \sum_k \sum_h a_{k,1} i_{h,k} \tag{27}$$

The above charge balance assumes that faradaic reactions are the only electrode processes; double layer charging is neglected.

3 GAS PHASE TRANSPORT

The gaseous reactants enter the fuel cell through the gas channels and are transported through the diffusion media into the catalyst layers where they react. Some gases may dissolve into the membrane and leak across the cell to react at the opposite electrode, thereby reducing the electrical work delivered by the fuel cell. The transport of the gases across the membrane is discussed later; here, only true gas phase mass transport is considered. Thus, the regions of interest are the diffusion media and the catalyst layers. Gas phase mass transport limitations may become important at the anode, the cathode, or both. These limitations could have severe effects on the operation of the fuel cell, as was shown with the introductory model.

Diffusion describes the movement of a given species relative to the motion of other species in a mixture. Several important modes of diffusion are ordinary (molecular), Knudsen, configurational, and surface diffusion. Ordinary diffusion almost always occurs; Knudsen diffusion is important in small pores; configurational diffusion takes place when the characteristic pore size is on the molecular scale; and surface diffusion involves the movement of adsorbates on surfaces. In a typical fuel cell, the pores are large enough that configurational diffusion does not occur. Surface diffusion may play an important role in interfacial reactions, but it is not treated in this chapter.

3.1 Ordinary diffusion

Fick's law may be used to describe the molecular movement of a dilute component in a mixture

$$\frac{\mathbf{N}_i}{\varepsilon} = -D_i c_{\mathrm{T}} \nabla x_i \tag{28}$$

where $\mathbf{N}_i$ is the superficial flux density of species i, ε is the porosity, D_i is the Fickian diffusion coefficient of species i in the mixture, which varies inversely with pressure and to approximately the 1.81 power with absolute temperature,[2] and c_{T} is the total concentration or molar density, which is assumed constant. Since we are discussing single phase phenomena, we have dropped the subscript k identifying the phase in the above and subsequent equations. In more concentrated and multicomponent systems, where it is necessary to take into account mutual interactions among different species, the generalized Stefan–Maxwell equations for constant temperature and pressure are appropriate

$$c_i \nabla \mu_i = \frac{RT}{c_{\mathrm{T}}} \sum_{j \neq i} \frac{c_i c_j}{D_{i,j}} (\mathbf{v}_j - \mathbf{v}_i) \tag{29}$$

where c_i is the concentration of i, μ_i is the chemical potential of i, $D_{i,j}$ is the binary interaction parameter between i and j, and $\mathbf{v}_i$ is the interstitial velocity of i relative to some reference velocity. As long as the reference frame is applied consistently, it need not be specified. The reason for this is that the frictional interactions depend only the relative and not the absolute values of the velocities. These equations involve only binary interaction parameters, and yield the correct number of transport coefficients as determined by species analysis.

Using the relationship between flux density and velocity

$$\frac{\mathbf{N}_i}{\varepsilon} = c_i \mathbf{v}_i \tag{30}$$

equation (29) can be rewritten, and for ideal mixtures at constant pressure and temperature, the Stefan–Maxwell equations take the form

$$\nabla x_i = \sum_{j \neq i} \frac{x_i \mathbf{N}_j - x_j \mathbf{N}_i}{\varepsilon c_{\mathrm{T}} D_{i,j}} \tag{31}$$

where x_i is the mole fraction of i. By the Onsager reciprocal relationships or by Newton's third law of motion, $D_{i,j} = D_{j,i}$. Bird *et al.*[2] provide correlations of $D_{i,j}$ for various gas pairs. Since the transport is occurring in pores, the diffusion coefficients need to be corrected for tortuosity. Frequently, a Bruggeman[15] equation can be used for this correction

$$\tau = \varepsilon^{-0.5} \tag{32}$$

The diffusion coefficients do not need to be corrected for porosity since it was explicitly accounted for by using interstitial properties and superficial fluxes.

The above set of equations yields $N - 1$ independent equations. In addition to determining the velocities of species relative to one another, the reference velocity must be determined, either by fluid dynamics or by the fixing the movement of a particular species with a properly chosen reference frame.

3.2 Knudsen diffusion

As the pore size decreases, molecules collide more often with the pore walls than with each other. This movement, intermediated by these molecule-pore-wall interactions, is known as Knudsen diffusion, named after the first person to study this type of flow comprehensively.[21] Knudsen diffusion occurs when the mean free path of the molecule is on the same order as the diameter of the pore. Using the kinetic theory of gases to express the mean free path of the molecule, the Knudsen diffusion coefficient is given by

$$D_{K_i} = \frac{d}{3}\left(\frac{8RT}{\pi M_i}\right)^{1/2} \tag{33}$$

where d is the pore diameter and M_i is the molecular weight of i. This diffusion coefficient is independent of pressure whereas ordinary diffusion coefficients have an inverse dependence on pressure.

Knudsen diffusion and ordinary or Stefan–Maxwell diffusion may be treated as mass transport resistances in series, and combined to yield

$$\nabla x_i = -\frac{\mathbf{N}_i}{\varepsilon c_{\mathrm{T}} D^e_{K_i}} + \sum_{j \neq i} \frac{x_i \mathbf{N}_j - x_j \mathbf{N}_i}{\varepsilon c_{\mathrm{T}} D^e_{i,j}} \tag{34}$$

where the superscript e indicates that the diffusion coefficients have been corrected for tortuosity. In effect, the pore wall, with zero velocity, constitutes another species with which the diffusing species interact, and it determines the reference velocity used for diffusion. From an order of magnitude analysis, when the mean free path of a molecule is less than 0.01 times the pore diameter, bulk diffusion dominates, and when it is greater than 10 times the pore diameter, Knudsen diffusion dominates. This means that Knudsen diffusion should be considered when the pore diameter is less than 100 nm at atmospheric conditions. For reference, a typical carbon diffusion medium has pores between 100 nm and 20 μm[22] in diameter and a catalyst layer contains pores on the order of 50 nm in diameter.[9]

3.3 Pressure driven flow

In most porous systems, the full Navier–Stokes equations are not solved; instead, a simplified construct is used. The reason for this simplification is that the actual porous structure is often unknown and a volume average approach is taken. This averaging is not valid over a bimodal distribution.[23] The convective flow encountered in a fuel cell is mainly pressure driven. If we further assume that the flow is steady and laminar (i.e., creeping flow), then we may use Darcy's law

$$\mathbf{v} = -\frac{k}{\mu}\nabla p \tag{35}$$

where $\mathbf{v}$ is the superficial mass average velocity, μ is the viscosity, and k is the permeability coefficient or Darcy's constant. The permeability coefficient is best determined from experiment, but should be on the order of the reciprocal of the square of the pore diameter. The Carman–Kozeny equation may be used to estimate the permeability[23]

$$k = \frac{\varepsilon^3}{(1-\varepsilon)^2 k' S_{\mathrm{o}}^2} \tag{36}$$

where S_o is a shape factor defined as the surface area to volume ratio of the solid phase and k' is the Kozeny constant, which has a value of approximately 5. If desired, equation (35) can be written as a flux in the absence of diffusion by using equation (30).

3.4 Combined transport

The inclusion of Knudsen diffusion coefficients is analogous to imposing a frictional interaction between each species in the gas mixture and the pore wall. When the characteristic pore diameter is small enough that the frictional interactions between gas species and pore wall are of the same order as, or larger than, the Stefan–Maxwell frictional interactions, then the reference velocity, which is necessary to specify the absolute velocities of all the species in the mixture, is set by fixing the velocity of the solid pore wall in the laboratory reference frame. In such a case, the inclusion of the Knudsen diffusion coefficients is mathematically similar to including a species $N + 1$ to represent the static pore wall in an N-component gas mixture. As mentioned above, the matrix of Stefan–Maxwell equations is not linearly independent, so one row must be removed and replaced with the specification of the reference velocity. In the case where Knudsen diffusion coefficients interact significantly with the remaining gas phase species, the reference velocity is that of the pore wall.

As the pore diameter becomes larger, however, the frictional interactions between the solid pore wall and the diffusing gas species become weaker and the coupling between them tenuous. In this case, the pore wall ceases to interact significantly with the diffusing gas species, and the interactions become too weak for the pore wall to specify the reference velocity. In such a case, one must resort to the original $N \times N$ matrix of Stefan–Maxwell relations, which becomes, in the absence of significant frictional interactions between the species and the pore wall, a singular matrix. In such a case, a single row of the matrix of equations is removed in order to specify a different reference velocity, namely, the mass average velocity of the gas mixture given by Darcy's law. The inclusion of Knudsen diffusion and bulk flow in the Stefan–Maxwell framework is discussed at great length by Mason and Malinauskas.[24]

4 LIQUID PHASE TRANSPORT

The transport of liquid water is an important consideration in the design of fuel cells intended to operate below 100 °C.[25] In a PEM fuel cell, for example, water may be transported as both a liquid and a gas. In general, the exchange between the two may be given by a kinetic expression for the evaporation rate. However, equilibrium between the pure liquid and the water vapor can often be assumed

$$x_{H_2O} = \frac{p^{vap}}{p} \tag{37}$$

where x_{H_2O} is the mole fraction of water in the vapor phase and p^{vap} is the vapor pressure of water, a strong function of temperature. Additionally, if the pores are small, it may be necessary to apply the Kelvin equation to correct the activity of water for curvature effects.[23]

Darcy's law, using the gradient of the liquid pressure as the driving force, may be used to describe the bulk transport of liquid water in the gas diffusion media and catalyst layers. These media are typically unsaturated, introducing an additional complication because the permeability is typically a strong function of the saturation level. Frequently, a power law relationship holds between permeability and the saturation level[23]

$$k = k_{sat} S^m \tag{38}$$

where k_{sat} is the permeability at complete saturation, S is the saturation level, and the exponent m usually has a value of approximately 3. The saturation is defined as the fraction of the pore volume filled with liquid. When a measured value for k_{sat} is unavailable, the Carman–Kozeny equation can be used to make an estimate. The saturation is often related through porosimetry data to the capillary pressure, p_c, which is defined as the liquid pressure minus the gas pressure. The capillary pressure is related to the pore diameter by[23]

$$p_c = -\frac{4\sigma \cos\theta}{d} \tag{39}$$

where σ is the surface tension, d is the pore diameter, and θ is the contact angle, which is related to the hydrophobicity of the pore.

5 ELECTROLYTIC AND MEMBRANE PHASE TRANSPORT

To model the behavior of a PEM fuel cell system, the transport of protons across the membrane must be described. It is the movement of protons that carries current and thus permits fuel cell operation. In order to relate current density to potential drop across the membrane, the flux of charged species resulting from a potential gradient in an electrolytic solution has to be expressed. In this section, we examine the frameworks of dilute solution theory and concentrated

solution theory, and examine the limitations of each. The complications of water transport due to electroosmotic drag are specifically considered, and the challenges of describing pressure driven flow in a solid polymer electrolyte are discussed.

5.1 Dilute solution theory

The simplest way to describe the movement of charged species in an electrolytic medium is by dilute solution theory. In dilute solution theory, one considers an uncharged solvent, charged solute species, and (perhaps) uncharged minor components. The superficial flux density of each dissolved species in terms of its interstitial concentration is given by:

$$\frac{\mathbf{N}_i}{\varepsilon} = -z_i u_i^e F c_i \nabla\Phi - (D_i^e + D_a)\nabla c_i + \frac{c_i \mathbf{v}}{\varepsilon} \qquad (40)$$

where $\mathbf{N}_i$ is the superficial flux density of species i. The first term in the expression is a migration term, representing the motion of charged species that results from a potential gradient. The migration flux is related to the potential gradient ($-\nabla\Phi$) by the charge number of the species z_i, its concentration c_i, and the tortuosity corrected mobility of the species u_i^e. The second term relates the diffusive flux to the concentration gradient and the Fickian diffusion coefficient D_i^e, which has been corrected for tortuosity. D_a is a dispersion coefficient representing the effect of axial dispersion. Strictly speaking, it is not a transport property and depends on fluid flow parameters; it disappears when convection is absent. Dispersion is usually ignored due to the relatively low velocities found in fuel cells. The final term is a convective term and represents the motion of the species as the bulk motion of the solvent carries it along. In general, the velocity of the solvent, $\mathbf{v}$, is determined by mass and momentum balances, e.g., by the Navier–Stokes equation. But as discussed above, in a porous network it is often easier to use Darcy's law.

Dilute solution theory considers only the interactions between each dissolved species and the solvent. The motion of each species is described by its transport properties, namely, the mobility and the diffusion coefficient. These transport properties can be related to one another at infinite dilution via the Nernst–Einstein equation:

$$D_i = RTu_i \qquad (41)$$

So long as the solute species are sufficiently dilute that the interactions among them can be neglected, material balances can be written based upon the above expression for the flux, and the concentration and potential profiles in the electrolyte can be determined. Neglecting dispersion, and using equation (41) and the definition of the current

$$\mathbf{i} = F\sum_i z_i \mathbf{N}_i \qquad (16)$$

equation (40) can be rewritten as a modified version of Ohm's law

$$\mathbf{i} = -\kappa\nabla\Phi - F\sum z_i D_i^e \nabla c_i \qquad (42)$$

where κ is the conductivity, defined as

$$\kappa = F^2 \sum_i z_i^2 u_i^e c_i = \frac{F^2}{RT}\sum_i z_i^2 D_i^e c_i \qquad (43)$$

The velocity does not appear in equation (42) due to electroneutrality, or, in other words, the bulk motion of a fluid with no charge density can contribute nothing to the current density.

5.2 Electroneutrality in the membrane

In PEM systems, in general, there is only one cation and one anion, the dissociated proton and the sulfonic acid site. The acid site is bound to the membrane, as seen in Figure 6 for the case of Nafion®. The sulfonic acid sites are distributed more or less evenly throughout the membrane, and, because the dissociation of the sulfonic acid groups is nearly complete in the presence of water, it is safe to assume that the charged acid sites are also distributed evenly throughout the membrane in the presence of water. Electroneutrality holds across the membrane

$$\sum_i z_i c_i = 0 \qquad (25)$$

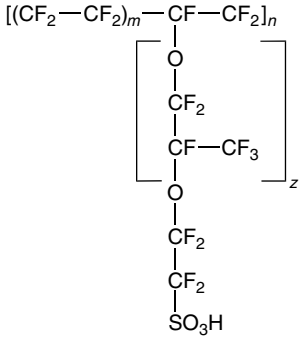

Figure 6. Schematic diagram of the structure of Nafion®. The value of z may be as low as 1, and the value of m ranges between 6 and 13.

except for a very thin double layer region near electrodes and other interfaces. Combining this equation with the requirement that the concentration of the anions be uniform across the membrane, it can be shown that the concentration of mobile protons is also fixed. In such a system, then, there will only be a migration and a convection term to describe the flux of other species, as is the case in a PEM based fuel cell system. If the details of the water concentration profiles and fluxes can be neglected in a well hydrated PEM fuel cell, Ohm's law can be used to relate the current density to the potential gradient in the membrane. Amphlett *et al*.[26] describe the performance of a fuel cell in this manner.

5.3 Water transport in the membrane

The framework of dilute solution theory allows for just two transport properties in a system composed of acid sites, protons, and water. If a model is to describe migration of protons, convective transport of water across the membrane, and electroosmotic drag, there must be a third parameter to quantify the fluxes. Furthermore, in most electrolytic systems, anions and cations move relative to a solvent whose velocity is determined by fluid dynamics. In the PEM fuel cell system, the anion sites are fixed, and the cations and water move relative to those sites. This peculiarity of having fixed acid sites changes the reference frame for transport in a PEM. Protons, water, and other minor species move relative to a fixed polymer framework, rather than all species moving relative to the convection of an aqueous solvent. The requirement that the anion species remain fixed in space is a key issue in describing transport in the membrane, and it results in the inclusion of the electrokinetic driving force.

Bernardi and Verbrugge[11, 27] use dilute solution theory to describe transport in the PEM system, for a system composed of a membrane, catalyst layer, and gas diffusion medium. The motion of the protons is related to the potential gradient and to the motion of the water in the membrane; the movement of the water is specified by pressure drop and electroosmotic drag:

$$\mathbf{v}_{H_2O} = -\left(\frac{k_p}{\mu}\right)\nabla p_L - \left(\frac{k_\Phi}{\mu}\right) z_f c_f F \nabla \Phi \qquad (44)$$

where k_p and k_Φ are the hydraulic permeability and the electrokinetic permeability, respectively, p_L is the hydraulic or liquid pressure, and z_f and c_f refer to the charge and concentration of fixed ionic sites, respectively.

The movement of water with the passing of current, even in the absence of a gradient of pressure or water activity, is known as electroosmotic drag and is an important factor in the design of fuel cell systems. Proper water management is critical for fuel cell operation (too much water leads to flooding at the cathode; too little water dries out the membrane and increases ohmic losses), so understanding the details of water transport is critical. Measurements of electroosmotic drag coefficients indicate that, near saturation, anywhere from 1 to 2.5 water molecules are dragged across the membrane with each proton.[28, 29] Electroosmotic drag delivers considerably more water to the cathode than stoichiometry dictates would be generated through the reduction of oxygen alone.

It is interesting to calculate the hydraulic pressure difference that, according to the above model, must be applied across the membrane to balance the electroosmotic drag with convection, and yield zero net water flux. When the net water flux is zero, the current density obeys Ohm's law. Combining this fact with equation (44) and assuming constant physical properties leads to the following expression:

$$\Delta p_L = \frac{k_\Phi z_f c_f F L i}{k_p \kappa_m} \qquad (45)$$

Thus, the required pressure difference is proportional to the current density and the thickness of the membrane, while it is inversely proportional to the conductivity of the membrane. In order to improve water management, it is common to operate with a higher pressure at the cathode than the anode.

5.4 Electrokinetic phenomena

There have been two principal approaches to describing the motion of water relative to the fixed polymer; the first is by the consideration of electrokinetic phenomena, and the second is the treatment of water as a dissolved species in the membrane. The treatment of electrokinetic phenomena, as Pintauro, Verbrugge, and others have adopted,[30, 31] is to describe the membrane as a series of pores with charged walls, through which liquid water filled with positively charged protons is allowed to move. The movement of the protons with the passing of current tends to drag water along with it, via the frictional interactions between the protons and the associated water. This approach presupposes that all the water in the membrane behaves as a fluid, and that there is a contiguous pore network that allows water to be transported from one side of the membrane to the other. In such a system, the movement of protons can be attributed to a potential gradient and a pressure gradient. The movement of water is determined primarily by a permeability of water subject to a pressure gradient, moving through the pore network. This approach is quite useful for describing fuel cell systems where the membrane is very well hydrated, but it requires that the water content be uniform across the

membrane, with only a pressure gradient as a driving force for water movement. Such a treatment does not necessarily lend itself to describing the flux of water resulting when there is a water activity gradient across the membrane.

The second approach, which treats all of the species as solute species absorbed in a single membrane phase, allows for a concentration gradient of water across the membrane. Thus, it can deal with issues of incomplete humidification of the membrane. The difficulty with this approach, however, is related to the details of pressure driven flow, which will be discussed later. The intricacies of Schroeder's paradox, namely, that the membrane takes up different equilibrium amounts of water when exposed to liquid water and to steam, complicate the picture even further.

5.5 Concentrated solution theory

Under the rules of concentrated solution theory, the framework for describing the transport of species is altered slightly from dilute solution theory. Instead of describing only the interactions between each solute species and the prescribed solvent, concentrated solution theory also describes the interactions of the species with each other; hence, it is more generally valid, especially for nonideal systems. In concentrated solution theory, a force balance is written that equates a thermodynamic driving force to a sum of frictional interactions. At constant temperature and pressure, the driving force is the gradient of electrochemical potential, and the frictional interactions are specified by the motion of the species relative to one another:

$$c_i \nabla \mu_i = \frac{RT}{c_T} \sum_{j \neq i} \frac{c_i c_j}{D^e_{i,j}} (\mathbf{v}_j - \mathbf{v}_i). \tag{46}$$

Here the $D_{i,j}$ term is a binary diffusion coefficient specifying the frictional interaction between species i and j. This equation is just a restatement of the generalized Stefan–Maxwell diffusion equation except now μ_i represents the electrochemical instead of chemical potential. Furthermore, as with Stefan–Maxwell diffusion, it may be necessary to choose explicitly a reference velocity, whether it is the velocity of a particular species, the mass average velocity, or the volume average velocity. For mass transport in the membrane, the membrane velocity is often used. The presence of a high molecular weight polymer is allowable under the Stefan–Maxwell framework. The diffusion coefficients are determined from experimental measurements. An appropriate choice of concentration scale is necessary to interpret the measurements and assign values to the diffusion coefficients; as long as the assumptions about the molecular weight of the polymer are applied consistently to both data analysis and system modeling, the framework will hold.

In a multicomponent system composed of N species, there are $N(N-1)/2$ independent transport properties. For a system composed only of protons, acid sites, and water, the framework of concentrated solution theory specifies three transport properties: the membrane-proton binary diffusion coefficient, the water-proton binary diffusion coefficient, and the water-membrane binary diffusion coefficient. These three coefficients can be arranged to yield the ionic conductivity of the membrane, the electroosmotic drag coefficient of water, and the diffusion coefficient of water in the membrane.

Concentrated solution theory has been used to describe transport in fuel cell membranes.[12, 32] By careful inversion of the Stefan–Maxwell equations in special cases (e.g., in the absence of current or in the absence of a water activity gradient) $D_{i,j}$ can be related to measurable transport properties; namely, D_{H_2O}, the diffusion coefficient of water; κ, the ionic conductivity; and ξ, the electroosmotic drag coefficient, which is the number of water molecules carried across the membrane with each hydrogen ion in the absence of a water activity gradient. Re-casting the Stefan–Maxwell equations in terms of these properties, we find[33]

$$\mathbf{i} = -\frac{\kappa \xi}{F} \nabla \mu_{H_2O} - \kappa \nabla \Phi \tag{47}$$

$$\mathbf{N}_{H_2O} = -\left(D_{H_2O} + \frac{\kappa \xi^2}{F^2} \right) \nabla \mu_{H_2O} - \frac{\kappa \xi}{F} \nabla \Phi \tag{48}$$

The multicomponent diffusion equation may be combined with the material balance equations and the condition of electroneutrality to provide a consistent description of transport processes in concentrated electrolytic systems.

5.6 Pressure driven flow in the membrane

In order to describe the effect of a pressure gradient on the transport of species in a membrane, it has been proposed that the electrochemical potential gradient be replaced with a more generalized driving force, suggested by Hirschfelder, Curtiss, and Bird[34]

$$d_i = c_i \left[\nabla \mu_i + \overline{S_i} \nabla T - \frac{M_i}{\rho} \nabla p - \boldsymbol{X}_i + \frac{M_i}{\rho} \sum_j \boldsymbol{X}_j c_j \right] \tag{49}$$

where d_i is the driving force per unit volume acting on species i, M_i is the molecular weight of species i, $\overline{S_i}$ is the molar entropy of species i, ρ is the density of the solution, and the $\boldsymbol{X}_i$ terms refer to body forces per mole

acting on species i. Bennion[35] applies this treatment to a membrane by requiring that the stresses acting on the membrane constitute the external body force $\boldsymbol{X}_i$, a force that is absent for the solid species. If there is only a single body force acting, then a mechanical force balance requires that

$$c_m \boldsymbol{X}_m = \nabla p \tag{50}$$

This relationship allows one to simplify the above driving force for a membrane.

In general, for a species containing N solute species, there are $N + 3$ variables that must be determined: N compositional variables, the potential (Φ), the temperature, and the pressure. Either by the energy balance or by the requirement of isothermal conditions, the temperature profile can be determine, and N material balances, then, will allow for the concentration profiles to be solved. The requirement of electroneutrality provides an additional equation for the potential. Thus, there is required one additional equation to determine the pressure drop.

In Pintauro and Bennion's[36] development, they back off from this framework and, in a treatment of desalinization, consider a membrane equilibrated with liquid water and exposed to NaCl solutions. They write a matrix that relates fluxes of water, current, and NaCl salt to driving forces in pressure, electrolyte concentration, and potential. Assuming uniform water content, they solve for the relevant variables by material balances on water and salt concentration, and by electroneutrality. The implicit assumption of uniform water content also forces them to consider the membrane as a separate phase, thereby allowing the Gibbs-Duhem equation to specify the chemical potential of the water, rather than allowing for an additional degree of freedom.

Meyers[37] addresses the problem from a slightly different perspective. He assumes that the water and ion content of the membrane is all part of a single, homogeneous phase. He argues that in a single phase system, a pressure gradient cannot be supported because there is nothing to withstand the force; a pressure gradient should impose net movement of the membrane itself. He treats pressure driven flow by allowing for a discontinuity in pressure at the membrane/solution interface, and argues that additional mechanical stresses compressing the membrane should be indistinguishable from the thermodynamic pressure. In his treatment, the thermodynamic pressure might be discontinuous, as the total force acting on the membrane consists of a liquid solute pressure combined with the mechanical stress of the solid structures (gas diffusion media, flow fields, etc.) that support the membrane. Equilibrium is imposed on all soluble species by requiring equality of electrochemical potential of all soluble species at the membrane/solution interfaces.

Since the PEM in a fuel cell is not always saturated with water, the uptake of water at lower activities needs to be considered. If, as seems likely, acid sites do not induce condensation of bulk-like water in the pores over the entire range of water activities that a fuel cell is likely to experience, then the behavior of water that is associated strongly with the membrane must be treated and is not bulk-like. While some of the water in a well hydrated membrane might behave similarly to liquid water collected in open pores, at lower water content, the water behaves more like a solute species dissolved in the membrane.

For a fuel cell system that is not completely hydrated, the strong dependence of ionic conductivity on water content[38] demands that careful attention is paid in determining the concentration profile of water in the membrane; this profile, in turn, has a strong effect on the ohmic losses in the membrane. Perhaps the true nature of PEMs is one that contains elements of both models: a phase that specifically absorbs some water and imparts low levels of ionic conductivity and a second phase that behaves primarily like bulk water. These two approaches have not, as of yet, been reconciled into an overarching, complete theory of membrane transport that addresses all of the relevant issues.

5.7 Transport properties

Regardless of the details of model construction, reliable data on transport properties are necessary to quantify transport in PEMs. Perfluorosulfonate membranes with structures like that shown in Figure 6, including Nafion®, have been characterized fairly extensively. The ionic conductivity is generally measured by ac impedance techniques,[39] and all of the models described above rely on conductivity data to predict ohmic losses. The saturation of the membrane can affect the conductivity and transport properties greatly, and thus these effects must be taken into account. Furthermore, the thickness can also appreciably affect the transport properties.[40]

Fuller and Newman[28] devised a technique to measure the electroosmotic drag coefficient of water in a PEM by relating the drag coefficient to the open-circuit potential difference measured across a membrane with different water concentrations in the membrane sections adjacent to the two electrodes. This technique was repeated by researchers at Los Alamos,[29] who also reported on volumetric measurements performed on a membrane exposed to liquid water. Water diffusion coefficients have proved difficult to measure in the PEM system, although they have been estimated by NMR techniques.[41] Also of interest are molecular simulations to calculate the transport properties of perfluorosulfonate membranes from *ab initio* electronic structure calculations and dielectric continuum modeling.[42]

5.8 Transport of uncharged species in the membrane

In general, the transport of additional uncharged species is neglected in the models presently available in the open literature. There are exceptions; notably, Bernardi and Verbrugge[11] discuss the crossover of hydrogen and oxygen in their paper, treating the transport of the gases by convection and diffusion in the steady state. Springer *et al*.[43] discuss the importance of the diffusion of hydrogen and oxygen in the membrane and note that transport of these species appears to be much higher in the catalyst layers of the membrane electrode assembly (MEA) than would be expected from measurements of crossover through a membrane separator.

One system in which the movement of uncharged species is particularly important is the direct methanol fuel cell (DMFC), where methanol crossover occurs and compromises fuel cell efficiency. Several models exist that describe methanol crossover.[44, 45] These models generally treat methanol as a minor species in the solution, transported by diffusion and convection along with the water that is present in much higher concentrations.

6 NUMERICAL SIMULATIONS

The complexity of the governing differential equations that we have outlined for modeling porous electrodes generally precludes analytic solution, and numerical simulations must be used. Numerical models lend themselves to the incremental inclusion of ever greater levels of detail, which cannot usually be said of analytic solutions. In fact, while it may be possible to reduce the number of variables through mathematical manipulation, this is often not the best course of action because it reduces the flexibility of the program. Furthermore, the increase in computation time is usually modest, at least for a one-dimensional model. When constructing a numerical model, it is best to include a complete picture of the cell sandwich in order to capture interactions among the various components. Thus, for example, a one-dimensional model of a PEM fuel cell could include the regions outlined in Figure 1.

A useful approach to numerical modeling of porous electrodes is as outlined below. Conservation equations are cast in control volume form, as depicted schematically in Figure 7. Patankar[46] describes this approach in detail. The integer j is the spatial mesh point, the integer n is the discretized time. Vectors are defined at half mesh points, while scalars are defined at full mesh points. Reaction terms are evaluated at quarter mesh points for each half mesh box. In the case of material balances, this approach

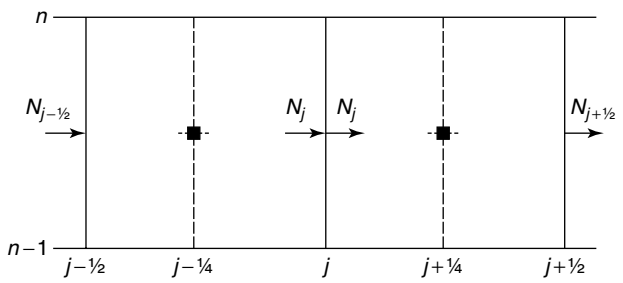

Figure 7. Schematic of the control volume approach for numerical simulations.

rigorously conserves mass, which cannot be said of finite difference methods. The coupled differential equations in the spatial domain may be solved with a banded solver, such as that described in Appendix C of Newman.[47] Crank-Nicholson time stepping, which involves averaging the equations symmetrically in time, is recommended in order to achieve stability and second order accuracy in time.

6.1 Cathode simulation

In this section, we present steady state results from a numerical model of the cathode of a PEM fuel cell. The model presented in this work is similar to that of Springer and co-workers[39, 43] and Perry *et al*.[48] Springer and coworkers demonstrated how to use a model like this to fit experimental data from lab-scale fuel cells. Perry *et al*. examined limiting cases due to either oxygen or ionic mass transport limitations within the catalyst layer. We have selected the cathode for our example because it is the most important electrode, in terms of polarization losses, in PEM fuel cells operating on either hydrogen or a reformed hydrocarbon fuel. A number of publications have dealt with simulations of the cathode and limiting cases that may arise under certain conditions. We discuss both of these topics in this section. Furthermore, we mention some of the diagnostic techniques that may be used to understand what is limiting the performance of a fuel cell electrode.

The model treats the diffusion of oxygen through the diffusion medium and the catalyst layer, ohmic drop in the ionomeric and solid phases within the catalyst layer, and oxygen reduction kinetics. Oxygen diffusion within the catalyst layer is treated with Fick's law, Ohm's law is used to describe the potential drop within the ionomeric and solid phases, and the ORR is assumed to follow Tafel kinetics with a first order dependence on the oxygen partial pressure and a cathodic transfer coefficient of 1. The total gas pressure and temperature are assumed constant. The model does not treat the water generated by the reduction of oxygen. Thus, the flow of water through the cathode

catalyst layer and the diffusion medium does not affect the oxygen transport. This is an important simplification that limits the applicability of a model of this type, since water management is a key to the proper design and operation of a PEM fuel cell. The conductivity of the ionomer within the catalyst layer is assumed to be constant, implying that the hydration level of the ionomer is uniform.

The model contains the following five variables: Φ_1, the potential in the solid phase; Φ_2, the potential in the ionomeric phase; i_1, the current density in the solid phase; i_2, the current density in the ionomeric phase; and x_{O_2}, the oxygen mole fraction. The interface between the membrane and the catalyst layer is located at $z = 0$, while the interface between the catalyst layer and the diffusion medium is located at $z = L$. The boundary conditions are

$$\Phi_2|_{z=0} = 0$$
$$\Phi_1|_{z=L} = V$$
$$i_1|_{z=0} = 0$$
$$i_2|_{z=L} = 0$$
$$\nabla x_{O_2}|_{z=0} = 0$$

and

$$x_{O_2}|_{z=L} = x_{O_2}^{b}\left(1 - \frac{i_1|_{z=L}}{i_{lim}}\right) \quad (51)$$

Thus, the ionomeric potential is arbitrarily set to 0 at $z = 0$, the solid phase potential is set at the interface between the catalyst layer and the diffusion medium, all of the current is carried in the ionomeric phase at the membrane interface, and all of the current is carried by the solid phase at the diffusion medium interface. The oxygen mole fraction at $z = L$ is set in accordance with a mass transfer resistance in the diffusion medium consistent with the limiting currents in Table 2. In this model, it is assumed that no oxygen diffuses past the interface between the catalyst layer and the membrane.

The simulations were run using a program written in FORTRAN using Newman's BAND(J), MATINV, and AUTOBAND subroutines.[47] The governing equations were cast in finite difference form.

Table 2 gives the parameters used in the simulations. These values are representative of state of the art PEM fuel cells. The interfacial area per unit volume was selected to give a catalyst surface area of $50\,m^2\,g^{-1}$. The exchange current density was selected to give a mass specific current density of $200\,mA\,mg_{Pt}^{-1}$ at a cathode potential of 0.9 V and an oxygen partial pressure of 1 bar. The value of the limiting current on air is typical for a PEM system and is assumed to be proportional to the oxygen mole fraction in the gas channel.

Table 2. Input and varied parameters used for the numerical simulations of a cathode under a base case, an ohmically limited case, and a mass transfer limited case.

Input parameters	
Temperature	65 °C
Total gas pressure	1 bar
Gas relative humidity	100%
Standard potential	1.195 V
Electrode thickness	10 μm
Platinum loading	$0.4\,mg\,cm^{-2}$
Cathodic transfer coefficient	1
Catalyst surface area	$50\,m^2\,g^{-1}$
Interfacial area per unit volume	$2.00 \times 10^5\,cm^2\,cm^{-3}$
Exchange current density	$1.51 \times 10^{-8}\,A\,cm^{-2}$
Limiting current (air)	$2.13\,A\,cm^{-2}$
Limiting current (oxygen)	$10.1\,A\,cm^{-2}$
Channel oxygen mole fraction (air)	0.16
Channel oxygen mole fraction (oxygen)	0.75
Variable parameters	
Base ohmic resistance	$1.00 \times 10^{-5}\,\Omega\,cm^2$
High ohmic resistance	$0.2\,\Omega\,cm^2$
Base oxygen diffusion coefficient	$2.30 \times 10^{-2}\,cm^2\,s^{-1}$
Low oxygen diffusion coefficient	$2.00 \times 10^{-4}\,cm^2\,s^{-1}$
Calculated parameters[a]	
Roughness factor	200
i (0.9 V,1 bar O_2)	$200\,mA\,mg_{Pt}^{-1}$
i (0.9 V,1 bar O_2)	$400\,\mu A\,cm_{Pt}^{-2}$

[a]Derived from Ref. [40].

Three cases are considered. Case 1, the base case, simulates a cathode with negligible ohmic drop and negligible oxygen mass transfer limitations within the catalyst layer. Case 2 describes a cathode with significant ohmic limitations, but negligible mass transfer limitations. Finally, case 3 simulates an electrode with negligible ohmic limitations, but significant mass transfer limitations within the catalyst layer. The parameters for cases 2 and 3 were selected to give similar polarization losses on air. The ohmically limited case may correspond to an electrode with a low ionomer content, while the mass transfer limited case may correspond to an electrode with a high ionomer content. In practice, there is probably a natural trade-off between ohmically limited electrodes and mass transfer limited electrodes.

Figure 8 shows polarization curves for the three cases on fully humidified air and oxygen. At low current densities, all of the electrodes are kinetically limited and perform similarly. As the current density increases, the polarization associated with the ohmic and mass transfer effects becomes significant, and the performance of the three electrodes on air begins to deviate. At a current density of $1\,A\,cm^{-2}$, the ohmic and mass transfer cases are approximately 50 mV below the kinetic case. All three cases have the same limiting current, corresponding to zero oxygen

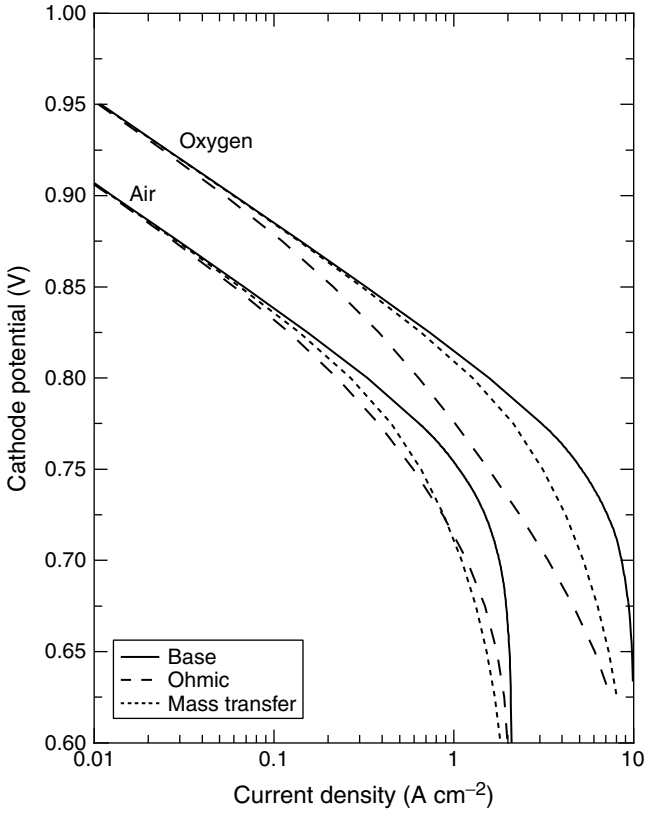

Figure 8. Polarization curves for the base, ohmically limited, and mass transfer limited cases of the cathode simulation for feeds of humidified air and oxygen. The base case is as given in Table 2, the ohmically limited case increases the ohmic resistance of the base case, and the mass transfer limited case decreases the oxygen diffusion coefficient of the base case.

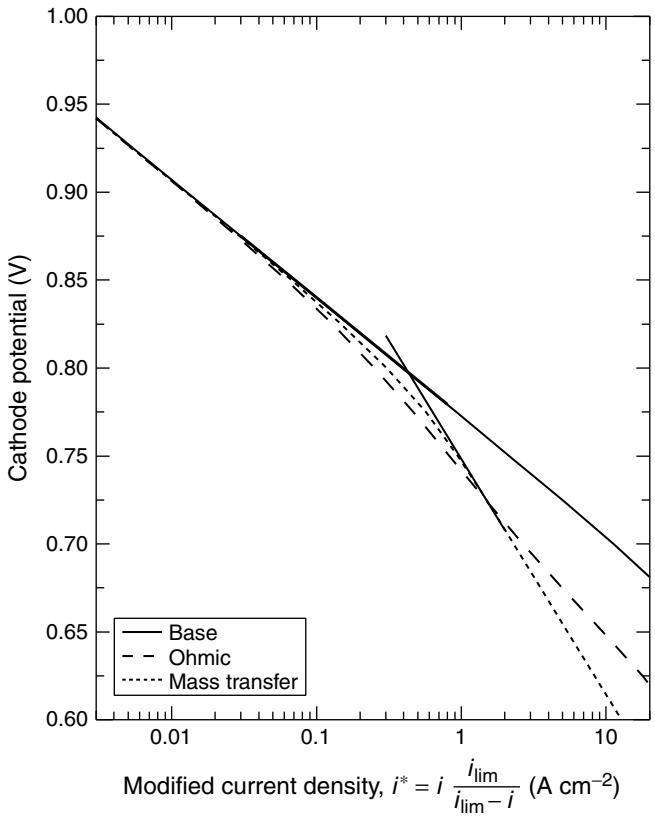

Figure 9. Polarization curves modified to remove external mass transfer effects for the three cases of the cathode simulation on air. The bold lines represent lines with single and double Tafel slopes.

partial pressure at the interface between the electrode and the diffusion medium.

The oxygen polarization curves are instructive. The ohmically limited electrode begins to deviate from the base electrode at the same current density on oxygen as it does on air. In the absence of external mass transfer limitations, the differences in potential between the base electrode and the ohmic electrode at a fixed current density would be identical for oxygen and air. The mass transport limited electrode, on the other hand, begins to deviate from the base electrode at the same cathode potential on oxygen as it does on air. In this case, the differences in current density between the base and mass transfer electrodes at a fixed cathode potential are the same for oxygen and air. Both of these results were reported by Perry *et al.*[48]

Figure 9 shows the cathode potential as a function of a mass transfer corrected current for the air simulations on all three electrodes. This type of plot corrects for external mass transport limitations, and allows for changes in the Tafel slope due to phenomena occurring within the catalyst layer to be seen more clearly. All three electrodes show a single Tafel slope at high potentials, as expected, since there are only kinetic limitations. This single slope extends through the entire potential range in the case of the kinetically limited electrode. The mass transfer electrode shows a distinct double Tafel slope at lower cathode potentials due to a non uniform reaction rate in the electrode caused by the strong mass transfer limitations. The ohmic electrode shows an increased slope, but not a double Tafel slope on this scale. Mass transport limitations internal to the catalyst layer are, in the absence of ohmic limitations, a function of potential, while ohmic limitations, in the absence of mass transfer limitations, are a function of current density. This explains why the double Tafel slope due to mass transfer limitations is visible on this plot while the double Tafel slope due to ohmic limitations is not. Thus, it may be possible to discern between mass transfer limited and ohmically limited electrodes by plotting data this way.

The difference in potential between the oxygen and air curves at a given current density, the oxygen gain, is simply

$$V_{O_2} - V_{air} = \frac{RT}{\alpha F} \ln\left(\frac{x_{O_2,ox}}{x_{O_2,air}}\right) \tag{52}$$

The oxygen gain increases with increasing current density as mass transport losses become more important, and it is larger for the mass transfer limited cathode than it is for either the ohmic electrode or the kinetic electrode. It can be shown that, in the absence of external mass transfer limitations, the oxygen gain for an ohmically limited system retains its value, while the oxygen gain for the mass transfer limited electrode doubles. Figure 10 elaborates on this point by plotting the ratio of current density measured on oxygen to the current density measured on air at the same cathode potential. This ratio is equal to $x_{O_2,ox}/x_{O_2,air} = 4.76$ for both the kinetic and mass transfer limited electrodes at all potentials. Thus, these electrodes show a first order dependence on oxygen concentration at all potentials. The ratio is 4.76 for the ohmically limited electrode at high potentials, where the electrode kinetics dominate. As the electrode potential drops, and the current density increases, the ratio falls, approaching the square root of 4.76 (line A in Figure 10). This behavior was explained by Perry *et al.*[48] At higher current densities, mass transport resistance in the diffusion medium, which is first order in oxygen, dominates, and the ratio again approaches 4.76. Thus, ohmic limitations within the electrode can lead to an apparent reaction order of 1/2, while mass transfer limitations may lead to an apparent reaction order of 1, with respect to oxygen.

Figures 11 and 12 show the current, potential, and oxygen distributions at 0.7 V on air for the ohmically limited and mass transfer limited electrodes, respectively. The current densities for these cases are approximately 1.1 and 1.2 A cm^{-2}, respectively. In the ohmically limited case, the reaction is shifted towards the interface between the membrane and the catalyst layer. The potential drop in the ionomer is about 70 mV, or approximately $L/(3\kappa)$. For reference, a value of $L/(2\kappa)$ is expected for a uniform current distribution. In the mass transfer limited case, the current is shifted towards the interface between the catalyst

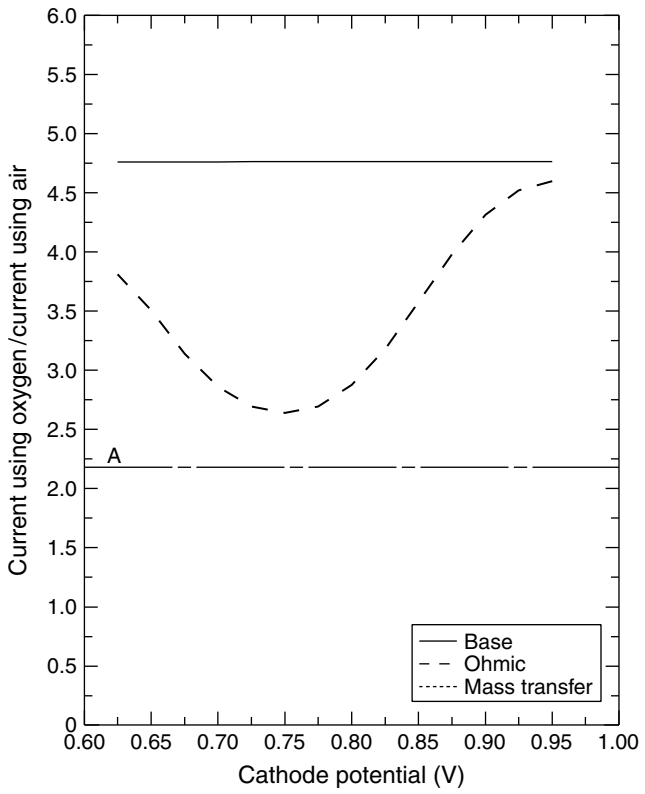

Figure 10. Ratio of current density measured on oxygen to the current density measured on air as a function of the potential of the cathode for all three cases of the cathode simulation. The mass transfer limited and base cases are the same, and equal the theoretical ratio for a kinetically or mass transfer limited electrode. Line A is the theoretical ratio for a completely ohmically limited electrode.

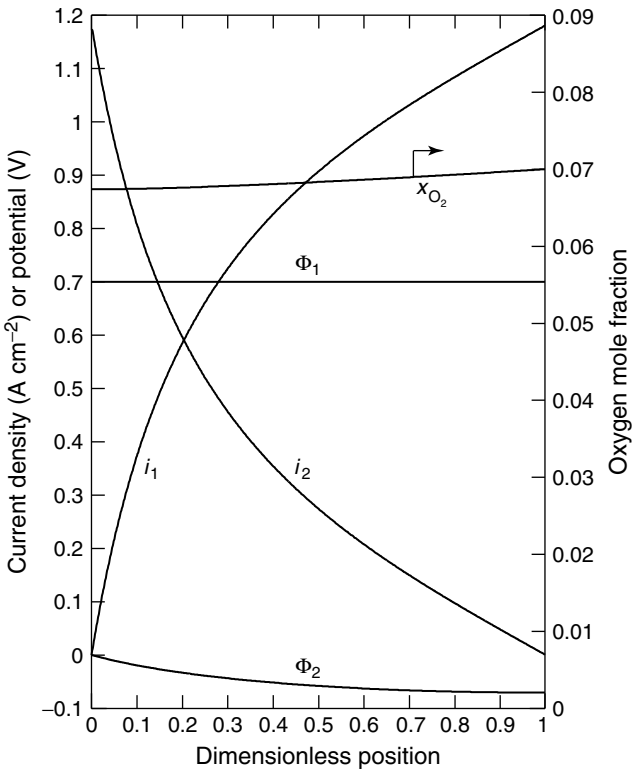

Figure 11. Potential, current density, and oxygen distributions in the solid and electrolyte phases of the cathode for the ohmically limited case. The cathode is at a potential of 0.7 V, and the feed is humidified air.

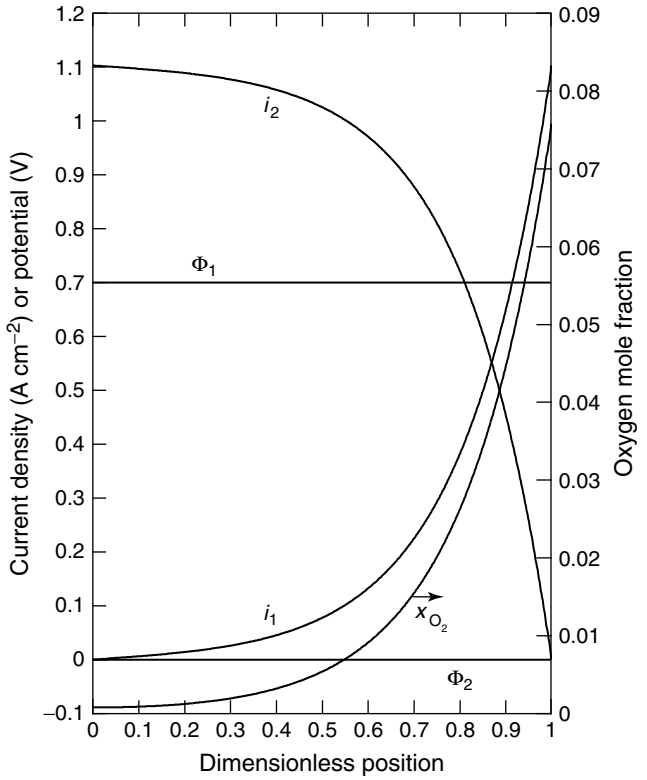

Figure 12. Current density, potential, and oxygen distributions in the solid and electrolyte phases of the cathode for the mass transfer limited case. The cathode is at a potential of 0.7 V, and the feed is humidified air.

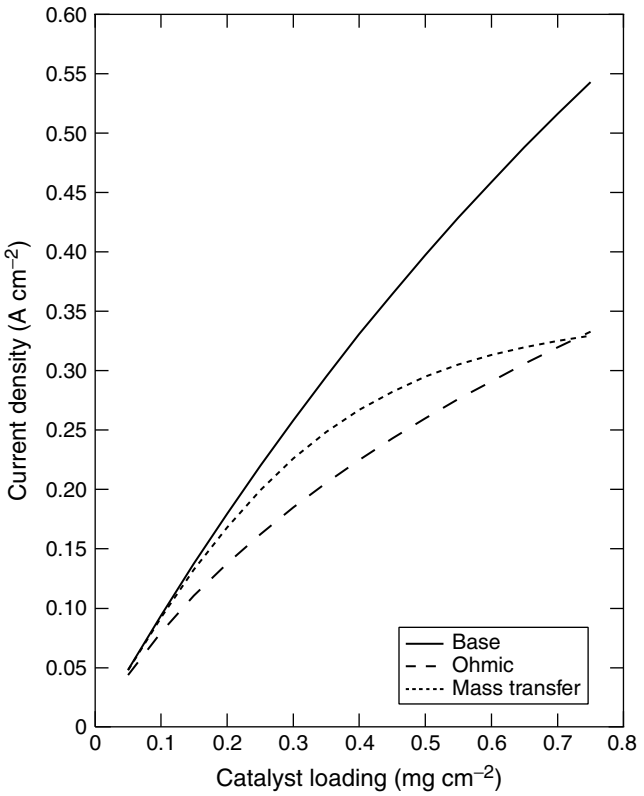

Figure 13. Effect of catalyst loading on current density at a cathode potential of 0.8 V and a feed of humidified air for all three cases of the cathode simulation.

layer and the diffusion medium; nearly all of the current is transferred between $z = 0.5$ and $z = 1$. These profiles agree with the double Tafel slope seen in Figure 9.

Figure 13 shows the effect of catalyst loading on air performance at a cathode potential of 0.8 V. The thickness of the catalyst layer was assumed to be proportional to the catalyst loading. If the catalyst were uniformly accessible, the result would be a straight line, but even the base case curves at high current densities because of the mass transfer resistance in the diffusion medium. The ohmic and mass transfer cases lose a significant amount of performance at high catalyst loadings. At very high loadings, the current in the mass transport limited electrode becomes independent of loading as the oxygen only penetrates a small region near the interface with the diffusion medium. Similarly, in the ohmically limited electrode, there is no advantage to increasing the loading beyond a certain point, as the ohmic limitations confine the reaction to a thin layer near the interface between the membrane separator and the catalyst layer. These limitations are clearly visible in Figures 11 and 12. Perry *et al.*[48] and Newman[47] present dimensionless groups that may be used to assess the importance of kinetic, ohmic, and mass transfer effects.

7 FUEL CELL MODELS

The cathode simulations described in the preceding section provide an introduction to the mathematical modeling of fuel cells, emphasizing the relationships between kinetic, mass transfer, and ohmic effects. The particular system was selected in order to yield interesting, important, and realistic results. Simple models like the one described in this work are useful as they can guide our thinking about the behavior of fuel cells. However, it is worthwhile to consider important additional effects that could be incorporated into a fuel cell model.

Consideration of an entire fuel cell cross-section represents an important advance since it allows one to examine interactions among the different layers. In the PEM case, communication of water between adjacent layers is of particular interest since proper water management is a key aspect of the design of PEM fuel cells. Bernardi and Verbrugge[11] treat the water balance in a fuel cell when the membrane is fully saturated at all times. The transport of liquid water through the various components is treated with Darcy's law, assuming constant permeabilities. Interestingly, in their simulations, the diffusion media are more

resistive to water flow than the Nafion® membrane. Since the porosities of the two components are reasonably similar, and the pores are probably significantly larger in the substrate than in the ionomer, this suggests that the saturation level of the substrate is quite low. A low saturation level is desired in the diffusion media in order to minimize the resistance to gas phase mass transfer.

Fuller and Newman[33] treat the water balance when the gas streams, and therefore, the membrane, are subsaturated. They use concentrated solution theory and their model solves explicitly for water and potential profiles in the membrane. Fuller and Newman integrated in the channel direction, following a procedure similar to the one described in this chapter. This allowed them to look at reactant depletion, water generation, and thermal effects. Nguyen and White[32] constructed a model in the channel direction applicable to cocurrent and countercurrent flow arrangements and examined various humidification schemes.

The models that we have focused on thus far involve a one-dimensional description of transport in the direction normal to the membrane. Two-dimensional effects may be important because the ribs in a fuel cell usually occlude part of the membrane. Kulikovsky *et al.*,[49] among others, have modeled this behavior. Finally, if uncoupling the different length scales is considered undesirable, full three-dimensional models can be pursued.[50]

8 CONCLUSIONS

In this chapter, we reviewed some of the models that have been developed to describe fuel cell performance. Even the simplest models provide some insight into the selection of proper operating conditions and, as such, can be very instructive tools. In designing a fuel cell, the details of mass transport within the layers of the cell should be examined. It is the interaction of several simultaneous processes, namely, ionic resistance, gas phase mass transport, kinetic losses, and liquid water removal, which make fuel cell operation possible. A detailed knowledge of these interrelated processes is necessary to develop a system that behaves optimally. It is perhaps worth noting that, were it possible to neglect completely any of these effects, one might conclude that the PEM fuel cell system is far from optimized. The fact that all of these effects must be considered in concert implies that the PEM fuel cell is nearly optimized for the present class of materials, as the improvement of one process often comes at the detriment of another. Modeling and analysis based upon the techniques reviewed in this chapter will assist fuel cell scientists and engineers to optimize fuel cells based upon the materials that will be the focus of future developmental efforts.

LIST OF SYMBOLS

Roman

a_i^{α}	activity of species i in phase α
$a_{k,p}$	interfacial surface area between phases k and p per unit volume, cm^{-1}
b	Tafel slope, V
c_i	concentration of species i per unit pore volume, $\mathrm{mol\ cm}^{-3}$
$c_{i,k}$	concentration of species i in phase k, $\mathrm{mol\,cm}^{-3}$
c_{T}	total solution concentration or molar density, $\mathrm{mol\,cm}^{-3}$
C	number of species
d	pore diameter, cm
d_i	driving force per unit volume acting on species i, $\mathrm{J\,cm}^{-4}$
D_i	Fickian diffusion coefficient of species i in a mixture, $\mathrm{cm}^2\,\mathrm{s}^{-1}$
D_{a}	dispersion coefficient, $\mathrm{cm}^2\,\mathrm{s}^{-1}$
$D_{i,j}$	diffusion coefficient of i in j, $\mathrm{cm}^2\,\mathrm{s}^{-1}$
D_{K_i}	Knudsen diffusion coefficient of species i, $\mathrm{cm}^2\,\mathrm{s}^{-1}$
f	the ratio of moles of inerts in the air stream to moles of inerts in the fuel stream
F_{a}	molar flow rate of carbon dioxide at the anode, $\mathrm{mol\,s}^{-1}$
F	Faraday's constant, $96487\,\mathrm{C\,eq}^{-1}$
$\mathbf{i}_k$	current density in phase k, $\mathrm{A\,cm}^{-2}$
i_0	exchange current density, $\mathrm{A\,cm}^{-2}$
$i_{h,k}$	transfer current density per unit interfacial area between phase k and the solid phase due to reaction h, $\mathrm{A\,cm}^{-2}$
i_{lim}	limiting current density, $\mathrm{A\,cm}^{-2}$
k	permeability, cm^2
k_{sat}	permeability measured at complete saturation, cm^2
k_{p}	hydraulic permeability, cm^2
k_{Φ}	electrokinetic permeability, cm^2
k'	Kozeny constant
L	catalyst layer thickness, cm
m	exponent in equation (38), usually equal to 3
M	number of degrees of freedom in equation (13)
M_i	molecular weight of species i, $\mathrm{g\,mol}^{-1}$
$M_i^{z_i}$	symbol for the chemical formula of species i in phase k having charge z_i
n_h	number of electrons transferred in electrode reaction h
N	number of species
$\mathbf{N}_i$	superficial flux density of species i, $\mathrm{mol\ cm}^{-2}\,\mathrm{s}^{-1}$
$\mathbf{N}_{i,k}$	flux density of species i in phase k, $\mathrm{mol\ cm}^{-2}\,\mathrm{s}^{-1}$

p total gas pressure, bar
p_i partial pressure of species i, bar
p_c capillary pressure, bar
p_L hydraulic or liquid pressure, bar
p^{vap} vapor pressure of water, bar
P number of phases in equation (13)
$r_{l,k-p}$ rate of reaction l per unit of interfacial area between phases k and p, mol s^{-1} cm^{-2}
$R_{g,k}$ rate of strictly homogenous reaction g in phase k, mol s^{-1} cm^{-3}
R' ohmic resistance, $\Omega\,cm^2$
R universal gas constant, 8.3143 J mol^{-1} K^{-1}
R number of equilibrated reactions in equation (13)
$s_{i,k,l}$ the stoichiometric coefficient of species i in phase k participating in reaction l
S saturation
S_o surface area to volume of solid phase, cm^{-1}
$\overline{S_i}$ molar entropy of species i, J mol^{-1} K^{-1}
t time, s
T absolute temperature, K
u hydrogen utilization
u_i mobility of species i, cm^2 mol J^{-1} s^{-1}
U reversible cell potential, V
U' potential intercept for the polarization equation, V
U^θ standard potential for oxygen reduction, 1.229 V at 25 °C
$\mathbf{v}_i$ interstitial velocity of species i, cm s^{-1}
V cell potential, V
W width perpendicular to flow in gas channel, cm
x_i mole fraction of species i
X_i extensive term referring to body forces per mole acting on species i
X_i ratio of moles of species i to moles of inerts in the same stream
y distance down the flow field channel, cm
z distance across the cell sandwich, cm
z_i valence or charge number of species i

Greek

α transfer coefficient for ORR
β symmetry factor
δ diffusion length, cm
ε porosity
ε_k volume fraction of phase k
Φ_1 potential in the solid phase, V
Φ_2 potential in the ionically conducting phase, V
η_s surface overpotential, V
κ conductivity of the electrolytic phase, S cm^{-1}
μ viscosity, g cm^{-1} s^{-1} or Pa s
μ_i chemical potential of species i in equation (29), J mol^{-1}
μ_i electrochemical potential of species i, J mol^{-1}
μ_i^α electrochemical potential of species i in phase α, J mol^{-1}
θ contact angle, degrees
ρ solution density, g cm^{-3}
σ surface tension in equation (39), N cm^{-1}
σ conductivity in the solid phase, S cm^{-1}
τ tortuosity
ξ electroosmotic drag coefficient

Subscripts

0 solvent or bulk value
1 solid, electronically conducting phase
2 ionic conducting phase
f fixed ionic site in the polymer membrane electrolyte
g homogeneous reaction number
h electron transfer reaction number
i generic species
j generic species
k generic phase
l heterogeneous reaction number
m membrane
p generic phase

Superscripts

0 inlet or initial value
b bulk value
e effective, corrected for tortuosity
i electrode interface value

REFERENCES

1. J. Newman, *Electrochim. Acta*, **24**, 223 (1979).
2. R. B. Bird, W. E. Stewart and E. N. Lightfoot, 'Transport Phenomena', 2nd edition, John Wiley & Sons, New York (2001).
3. J. Newman and W. Tiedemann, *AIChE J.*, **21**, 41 (1975).
4. Y. A. Chizmadzhev, V. S. Markin, M. R. Tarasevich and Y. G. Chirkov, 'Makrokinetika protsessov v poristykh sredakh (Toplivnye elementy)', Izdatel'stvo "Nauka", Moscow (1971).
5. J. Bockris and S. Srinivasan, 'Fuel Cells: Their Electrochemistry', McGraw-Hill, New York (1969).
6. J. S. Dunning, 'Analysis of Porous Electrodes with Sparingly Soluble Reactants', Unpublished Ph.D. Dissertation, University of California, Los Angeles, CA (1971).

7. J. Giner and C. Hunter, *J. Electrochem. Soc.*, **116**, 1124 (1969).
8. R. P. Iczkowski and M. B. Cutlip, *J. Electrochem. Soc.*, **127**, 1433 (1980).
9. M. Uchida, Y. Fukuoka, Y. Sugawara, N. Eda and A. Ohta, *J. Electrochem. Soc.*, **143**, 2245 (1996).
10. T. R. Ralph, G. A. Hards, J. E. Keating, S. A. Campbell, D. P. Wilkinson, M. Davis, J. St-Pierre and M. C. Johnson, *J. Electrochem. Soc.*, **144**, 3845 (1997).
11. D. M. Bernardi and M. W. Verbrugge, *J. Electrochem. Soc.*, **139**, 2477 (1992).
12. T. E. Springer, T. A. Zawodzinski and S. Gottesfeld, *J. Electrochem. Soc.*, **138**, 2334 (1991).
13. B. Pillay, 'Design of Electrochemical Capacitors for Energy Storage', Unpublished Ph.D. Dissertation, University of California, Berkeley, CA (1996).
14. J. Newman, *Ind. Eng. Chem. Res.*, **34**, 3208 (1995).
15. D. A. G. Bruggeman, *Ann. Phys.*, **24**, pp. 636 (1935).
16. K. Kinoshita, 'Carbon Electrochemical and Physiochemical Properties', John Wiley & Sons, New York (1988).
17. D. Bernardi, 'Mathematical Modeling of Lithium (Alloy) Iron Sulfide Cells and the Electrochemical Precipitation of Nickel Hydroxide', Unpublished Ph.D. Dissertation, University of California, Berkeley, CA (1986).
18. T. Springer, T. Zawodzinski and S. Gottesfeld, 'Modeling of Polymer Electrolyte Fuel Cell Performance with Reformate Feed Streams: Effects of Low Levels of CO in Hydrogen', Electrochemical Society, PV 97–13 (1997).
19. A. J. Appleby, *J. Electrochem. Soc.*, **117**, 328 (1970).
20. K. Kinoshita, 'Electrochemical Oxygen Technology', John Wiley & Sons, New York (1992).
21. M. Knudsen, 'The Kinetic Theory of Gases', Methuen, London (1934).
22. L. R. Jordan, A. K. Shukla, T. Behrsing, N. R. Avery, B. C. Muddle and M. Forsyth, *J. Appl. Electochem.*, **30**, 641 (2000).
23. F. A. L. Dullien, 'Porous Media: Fluid Transport and Pore Structure', Academic Press, New York (1979).
24. E. A. Mason and A. P. Malinauskas, 'Gas Transport in Porous Media: The Dusty-Gas Model', Elsevier, Amsterdam (1983).
25. D. M. Bernardi, *J. Electrochem Soc.*, **137**, 3350 (1990).
26. J. C. Amphlett, R. M. Baumert, R. F. Mann, B. A. Peppley, P. R. Roberge and T. J. Harris, *J. Electrochem. Soc.*, **142**, 1 (1995).
27. D. M. Bernardi and M. W. Verbrugge, *AIChE J.*, **37**, 1151 (1991).
28. T. F. Fuller and J. Newman, *J. Electrochem. Soc.*, **139**, 1332 (1992).
29. T. A. Zawodzinski, Jr, J. Davey, J. Valerio and S. Gottesfeld, *Electrochim. Acta*, **40**, 297 (1995).
30. P. N. Pintauro and M. W. Verbrugge, *J. Membr. Sci.*, **44**, 197 (1989).
31. A. G. Guzmán-Garcia, P. N. Pintauro, M. W. Verbrugge and R. F. Hill, *AIChE J.*, **36**, 1061 (1990).
32. T. V. Nguyen and R. E. White, *J. Electrochem. Soc.*, **140**, 2178 (1993).
33. T. F. Fuller and J. S. Newman, *J. Electrochem. Soc.*, **140**, 1218 (1993).
34. J. O. Hirshfelder, C. F. Curtiss and R. B. Bird, 'Molecular Theory of Gases and Liquids', John Wiley & Sons, New York (1954).
35. D. N. Benion, 'Mass Transport of Binary Electrolyte Solutions in Membranes, Water Resources Center Desalination Report No. 4', Tech. Rep. 66–17, Department of Engineering, University of California, Los Angeles, CA (1966).
36. P. N. Pintauro and D. N. Bennion, *Ind. Eng. Chem. Fundam.*, **23**, 230 (1984).
37. J. Meyers, 'Simulation and Analysis of the Direct Methanol Fuel Cell', Unpublished Ph.D. Dissertation, University of California, Berkeley, CA (1998).
38. T. A. Zawodzinski, Jr, T. E. Springer, J. Davey, R. Jestel, C. Lopez, J. Valerio and S. Gottesfeld, *J. Electrochem. Soc.*, **140**, 1981 (1993).
39. T. E. Springer, T. A. Zawodzinski, M. S. Wilson and S. Gottesfeld, *J. Electrochem. Soc.*, **143**, 587 (1996).
40. S. Srinivasan, D. J. Manko, H. Kock, M. A. Enayetullah and A. J. Appleby, *J. Power Sources*, **29**, 367 (1990).
41. T. A. Zawodzinski, Jr, M. Neeman, L. O. Sillerud and S. Gottesfeld, *J. Phys. Chem.*, **95**, 6040 (1991).
42. S. J. Paddison, R. Paul and T. A. Zawodzinski, Jr, *J. Electrochem. Soc.*, **147**, 617 (2000).
43. T. E. Springer, M. S. Wilson and S. Gottesfeld, *J. Electrochem. Soc.*, **140**, 3513 (1993).
44. K. Scott, W. Taama and J. Cruickshank, *J. Power Sources*, **65**, 159 (1997).
45. S. F. Baxter, V. S. Battaglia and R. E. White, *J. Electrochem. Soc.*, **146**, 437 (1999).
46. S. Patankar, 'Numerical Heat Transfer and Fluid Flow', McGraw-Hill, New York (1999).
47. J. S. Newman, 'Electrochemical Systems', Prentice Hall, Englewood Cliffs, NJ (1991).
48. M. L. Perry, J. Newman and E. J. Cairns, *J. Electrochem. Soc.*, **145**, 5 (1998).
49. A. A. Kulikovsky, J. Divisek and A. A. Kornyshev, *J. Electrochem. Soc.*, **146**, 3981 (1999).
50. A. Dutta, S. Shimpalee and J. W. Van Zee, *J. Appl. Electrochem.*, **30**, 135 (2000).